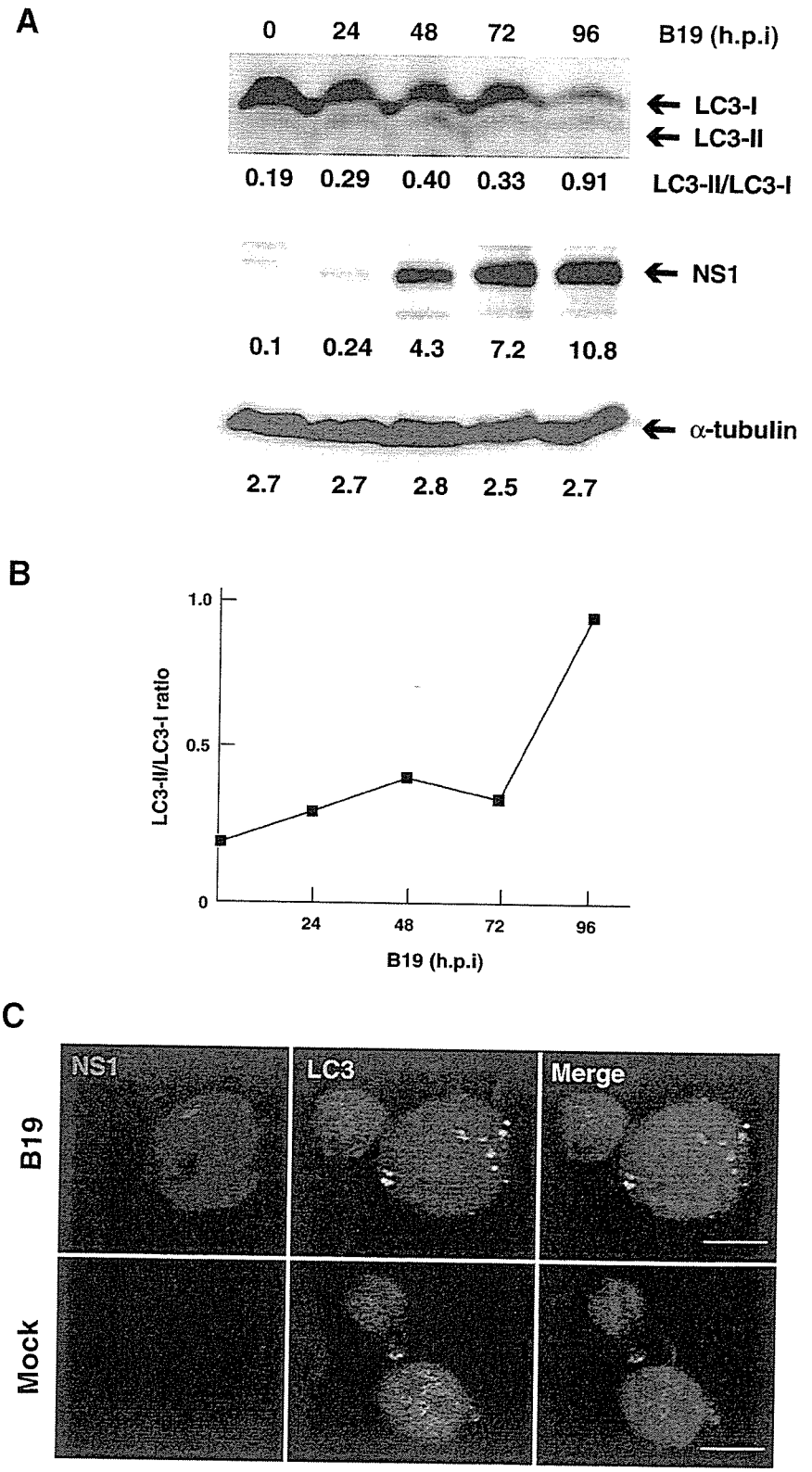

Fig. 3. Autophagy in B19-infected UT7/Epo-S1 cells. (A) Immunoblot analysis of LC3-II in cells infected with B19 virus at indicated times; 0, 24, 48, 72, and 96 h. The band intensities of endogenous LC3-I and LC3-II were quantified, and the LC3-II/LC3-I ratio is indicated. Band intensities for NS1 and α-tubulin are also shown. (B) The LC3-II/LC3-I ratio. Number calculated from panel A is shown. (C) Native LC3 expression in NS1-expressing cell. UT7/Epo-S1 cells were infected. B19 virus- or mock-infected cells were fixed and subjected to confocal microscopy analysis; NS1 staining (left panels), LC3 staining (middle panels) and merged images (right panels) of the same field are shown. Scale bars: 10 μm.

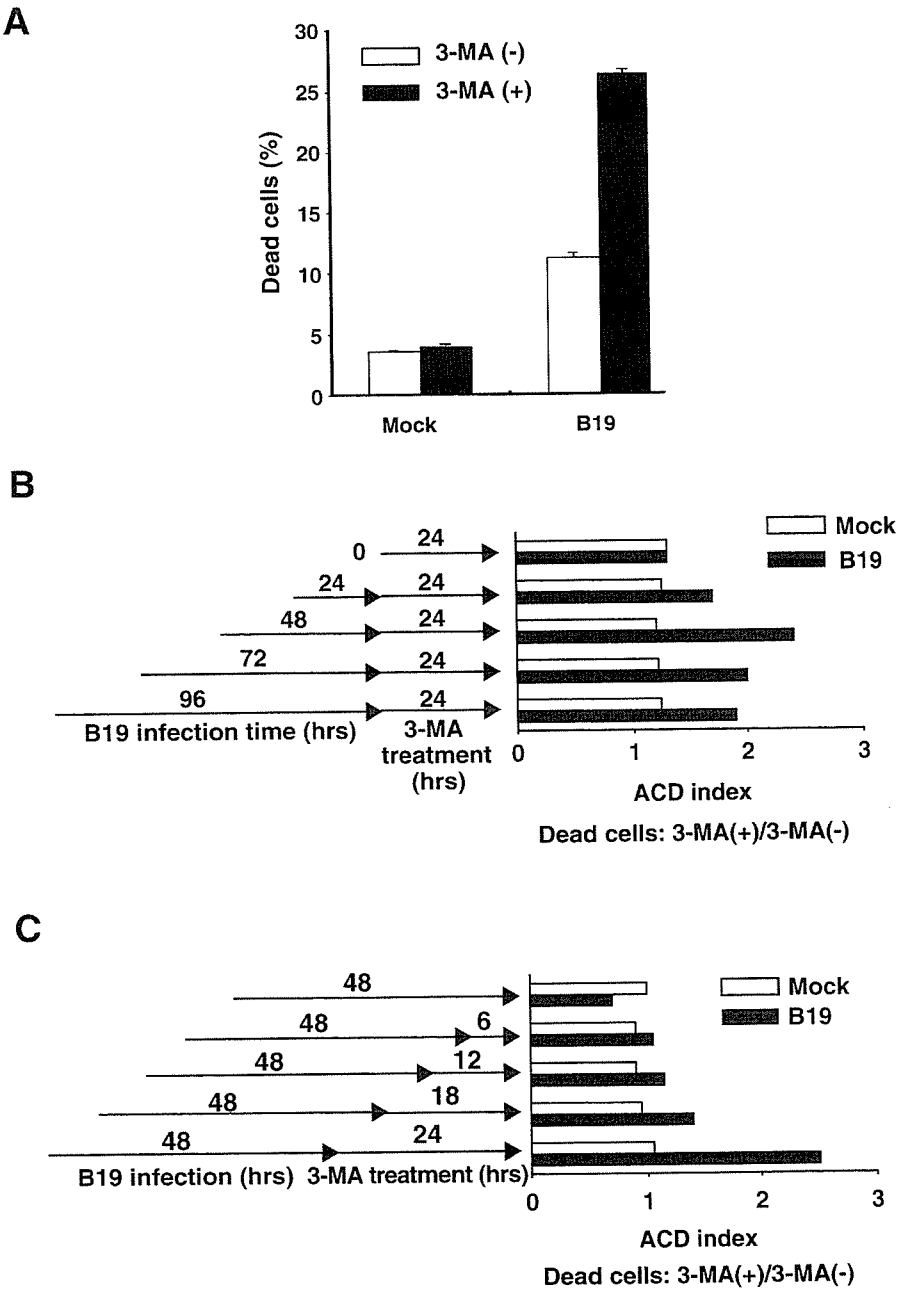

Fig. 4. The inhibitor of autophagy induces cell death in B19-infected cells. The percentages of dead cells were calculated with sub-G1 populations. (A) The percentage of dead cells treated with DMSO (open bars) or 5 mM 3-MA (solid bars) after 72 h post-infection. After the initial B19 infection for 48 h, cells were incubated in the presence of DMSO or 3-MA for additional 24 h. (B and C) UT7/Epo-S1 cells were infected with B19 virus (triangle) or mock (square). *Y*-axis indicates the ACD index, which is calculated by the ratio of dead cells in the presence and absence of 3-MA (3-MA(+)/3-MA(−)). (B) Kinetic analyses of ACD index on B19- or mock-infected cells. Cells were initially incubated in the presence or absence of B19 for 24, 48, 72, or 96 h, extensively washed, and then further incubated with or without 3-MA for 24 h. ACD index at the time point 0 was obtained from cells without infection and incubated with or without 3-MA for 24 h. (C) Kinetic analyses of ACD index on cells initially infected with B19 for 48 h. After the initial 48 h infection periods, cells were washed extensively and then cultured in the presence of 3-MA for indicated times on *X*-axis. Each experimental data represent from at least three independent experiments.

of its larger size and higher intracellular complexity, may be at least similar to the "cytopathic giant pronormoblasts" which appears among the B19 parvovirus inoculated normal bone marrow cells at 48 h after infection (Ozawa et al., 1987). Since no additional characteristics of the cytopathic giant pronormoblasts have been analyzed before, we could not fully distinguish the giant pronormoblasts found in bone marrow cells and the B19-B population in the UT7/Epo-S1 cells in the present study.

One interesting characteristics we found regarding the B19-B population is a profound G2-arrest phenotype (Fig. 1C). Cell cycle arrest status of B19-B was not only obvious by the FACS analysis but also evident in their severely retarded cell growth (Fig. 1D). Therefore, these B19-B cells are in good accordance with our former observation that B19 infection mediates cell cycle arrest at G2 phase with decreased cell viability (Morita et al., 2001).

We found that the cells from the B19-B population manifest significant morphological alternation compared with mock-infected cells (Figs. 2A, B). The swollen change was clearly identified in B19-infected cells and therefore can be interpreted as cytopathic effect. Although we formerly reported that B19 induces apoptosis (Yaegashi et al., 1999), cell enlargement is usually atypical. Since cell fate of the B19-B population should be either apoptosis or survival, we tested the former possibility. We found no characteristic observation found in apoptotic or necrotic cells, as judged by the permeability of mitochondria or plasma membrane (data not shown). We therefore conclude that the morphological alternation we found in the B19-B cells may be associated with their G2-arrest phenotype.

To our surprise, our EM analyses clearly revealed morphological characteristics within the cytoplasm. Organellas within the B19-infected enlarged cells, both on days 2 and 5, contained mitochondria which were at least partially degraded (Figs. 2Ah–l). Similar intracellular structures have been reported in sympathetic neurons after nerve growth factor (NGF) withdrawal (Kirkland et al., 2002). Mitochondria with EM-dark matrix have been interpreted as "matrix condensation", which have almost lost their proper definition, therefore appear as single-membrane structure containing EM-dense materials. We believe that our present study is the first report stating mitochondrial degeneration in B19-infected cells. In addition, it is of great interest that elimination of mitochondria is now shown to be at least partially mediated by cellular autophagy (Kissova et al., 2004). Further, a previous study demonstrated a coincidence between the onset of mitochondrial shrinkage (but not swelling) and the engulfment of mitochondria by autophagosomes (Tolkovsky et al., 2002). In this study, we clearly found that the degrading mitochondria were sequestrated by a double membrane structure, which is a hallmark of autophagosomes (Fig. 2Ak). To our knowledge, this study first reports the DNA virus-induced autophagy. Taken together with this notion, we conclude that B19-induced enlarged cells are actively engulfing mitochondria by way of cellular autophagy.

We also confirmed the induction of autophagy by biochemical analyses in B19-infected cells. Conversion of LC3, from cytoplasmic precursor LC3-I to lapidated and therefore autophagosomal resident LC3-II form, was clearly identified not only by Western blots but also by confocal microscopy (Figs. 3A and C). One characteristic feature of B19-induced autophagy is its appearance in the later time point after the infection, which seems to be the most at 48 to 96 h time points (Fig. 4B). This kinetics should be quite different from autophagy induced by nutrient starvation or the group A Streptococcus (GAS) infection, both of which are most apparent at least 3 to 6 h after the induction (Yoshimori, 2004). One explanation for the relatively late onset of autophagy is that some de novo synthesized viral protein may induce autophagy, while it may just be induced by general increase of cellular stress. To explore the former possibility, we tested whether NS1 induces autophagy, because NS1 expression seems to somewhat proceed the induction of autophagy (Figs. 3A and B). At present, however, we have obtained marginal induction of autophagy by NS1. We need to identify a mechanism by which B19 induces autophagy, such as other viral protein or cellular innate response against B19 infection.

Our present study demonstrated that autophagy induced by B19 mediates infected cell survival (Fig. 4A). At present, however, we do not have direct evidence for the precise biological significance of autophagy in B19-infected cells. One possibility is that infected cells inhibit B19 virus by sequestration the viral component, while another is that cells survive by mitochondrial breakdown and nutrient supply. NS1-expressed cells might result either from the use for virus replication or the destruction of the virus structure. In this context, it is interesting to see how other virus utilize autophagy. In RNA virus infection, such as poliovirus, RNA replication complexes co-localize with autophagosomes and thereby utilize the autophagic machinery for the virus replication. In the case of murine hepatitis virus (MHV), a member of the Coronaviridae, requires the autophagic pathway to form infectious virions, since the yield of extracellular virus is significantly diminished in clonal isolates of $Atg5^{-/-}$ mouse embryonic stem cells (Kirkegaard et al., 2004). Considering these RNA virus tactics to utilize the autophagy machineries, we speculate that B19 also may use autophagy for their propagation. If this hypothesis is correct, B19-infected cells treated with 3-MA may survive longer than non-treated cells, because B19 has an ability to induce apoptosis. Nevertheless, we found an opposite effect, indicating that autophagy rather facilitated cell survival. Regarding the B19-infected cell fate, we previously reported a typical kinetics, in which most of the infected cells get arrested at G2 phase within 12 h after the infection, then survive up to 72 h, and start dying accompanied with viral replication (Morita and Sugamura, 2002). In this study, we showed that inhibition of autophagy is most effective at 48 to 72 h after the infection, and thereafter decreases. Thus, autophagy seems to work during the initial 48–72 h after the B19 infection, probably in cells arrested at G2 phase, before they are competent for the virus replication. We speculate that whereas some enlarged cells fall into apoptosis following the G2-arrest, other enlarged ones manage to survive by activating the autophagy machinery. In other words, autophagy may benefit B19 allowing their expansion during the "time lag". To verify the hypothesis, we must overcome at least two major barriers. One is that, as far as we know, cell lines that are highly susceptible to B19 are limited. Second, little is known regarding the B19 expansion, from replication to release. To solve these problems, we need a cell line, which is highly propagative as well as highly susceptible to B19 infection.

Collectively, we first demonstrated that DNA virus infection induces autophagy. Autophagy induced by B19 contributed to cell survival, potentially leaving time periods for the viral replication and expansion. Further experiments are needed to explore the "fight" between the B19 and the host.

Material and methods

Cell line and chemicals

B19 virus antigen-positive human serum obtained from a blood donor was used as a B19 virus seed, the virus titer of

which was calculated to be 10^8 infectious units per milliliter by anti-VP1/2 immunostaining assays. UT7/Epo-S1 cells were inoculated with a multiplicity of infection of 10 with 20-fold-diluted virus seed at 10^6 cells/ml in Isocove's modified Dulbecco's medium (IMDM) and incubated for 2 h at 4 °C for virus adsorption. UT7/Epo-S1 cells, highly susceptible to B19 virus infection (Morita et al., 2001), were propagated in Isocove's modified Dulbecco's medium containing 10% fetal calf serum and 2 U/ml recombinant erythropoietin (Epo) (a gift from Kirin Brewery Pharmaceutical Research Laboratory, Tokyo, Japan). 3-Methyladenine (3-MA) was obtained from Sigma-Aldrich (Steinheim, Germany) and dissolved directly to the incubation medium.

Flow cytometry analysis

Cells were harvested, washed once and then resuspended in PBS solution containing 5 μg/ml propidium iodide (PI) and incubated at 37 °C for 30 min. Samples were then analyzed with a FACS Calibur flow cytometer using the Cell Quest software (BD Biosciences, Mountain View, CA).

Cell cycle analysis

Cell cycle analyses were performed as described previously (Darzynkiewicz et al., 1992). In brief, cells were infected with B19 virus and cultured for the indicated times. After the cells were washed twice with phosphate-buffered saline (PBS), they were suspended in propidium iodide (PI) solution (50 μg/ml PI, 0.1% sodium citrate, 0.2% NP-40, 0.05 mg/ml RNase), then incubated for 30 min at 4 °C. Cells in the sub-G1, G_0/G_1 and G_2/M fractions were counted with a FACScan fluorescence-activated cell sorter (FACS; BD Bioscience, Franklin Lakes, NJ). For some experiments, cells were infected with B19 for 24, 48, 72, or 96 h, and then washed with PBS three times. Subsequently, cells were further incubated with 5 mM 3-MA at 37 °C for additional 24 h. Dead cells including apoptosis were analyzed by flow cytometry, by determining the cells within sub-G1 fraction.

Western blotting

Whole-cell lysates were prepared with a lysis buffer (2% NP-40, 0.2% SDS in PBS supplemented with protease inhibitors). Western blot analyses were carried out as described previously (Nakashima et al., 2004). Anti-NS1 monoclonal antibody (MAb), ParC-NS1, specific for the NS1 C-terminal half of B19 virus (Morita et al., 2003), and anti-LC3 antibody against recombinant LC3 (Kabeya et al., 2000) were previously described. Anti-α-tubulin MAb (Sigma Aldrich Fine Chemicals, St. Louis, MO) was also purchased.

Electron microscopy

Cells were mock-infected, infected for 2 day or 5 day, and then washed once with 0.1 M cacodylate buffer, pH7.4. The cells were fixed with 2% glutaraldehyde in 0.1 M phosphate buffer. Subsequently, the rests of the procedure were conducted by Nissin EM Corp (Tokyo, Japan).

Immunocytochemistry

Immunocytochemistry was carried out as described previously (Morita et al., 2001). In brief, cells were fixed in 4% paraformaldehyde (PFA)–PBS for 15 min and labeled with following antibodies; anti-NS1 MAb antibody and anti-LC3 antibody. They were secondarily stained with Alexa Fluor 488 goat anti-mouse antibody and Alexa Fluor 594 goat anti-rabbit antibody (Molecular Probes, Inc., Eugene, OR). Confocal images of fluorescent materials in UT7/Epo-S1 cells were collected using a confocal laser scanning microscope, LSM510 META (Carl Zeiss, Oberkochen, Germany).

Acknowledgments

We gratefully acknowledge the gift of recombinant Epo from Kirin Brewery Pharmaceutical Research Laboratory, Tokyo, Japan. The authors thank Mr. Lamichhane Aayam for critically reading the manuscript. This work was supported in part by a Grant-in-aid for Scientific Research from the Japan Society for the Promotion of Science (JSPS), the 21st century Center of Excellence (COE) Program and Grant-in-aids for Scientific Research on Priority Areas from the Ministry of Education, Science, Sports, and Culture, a Grant-in-aid from the Ministry of Health, Labor, and Welfare of the Japanese Government. K.T. and M.K. are JSPS research fellows.

References

Darzynkiewicz, Z., Bruno, S., Del Bino, G., Gorczyca, W., Hotz, M.A., Lassota, P., Traganos, F., 1992. Features of apoptotic cells measured by flow cytometry. Cytometry 13 (8), 795–808.

Kabeya, Y., Mizushima, N., Ueno, T., Yamamoto, A., Kirisako, T., Noda, T., Kominami, E., Ohsumi, Y., Yoshimori, T., 2000. LC3, a mammalian homologue of yeast Apg8p, is localized in autophagosome membranes after processing. EMBO J. 19 (21), 5720–5728.

Kirisako, T., Ichimura, Y., Okada, H., Kabeya, Y., Mizushima, N., Yoshimori, T., Ohsumi, M., Takao, T., Noda, T., Ohsumi, Y., 2000. The reversible modification regulates the membrane-binding state of Apg8/Aut7 essential for autophagy and the cytoplasm to vacuole targeting pathway. J. Cell Biol. 151 (2), 263–276.

Kirkegaard, K., Taylor, M.P., Jackson, W.T., 2004. Cellular autophagy: surrender, avoidance and subversion by microorganisms. Nat. Rev., Microbiol. 2 (4), 301–314.

Kirkland, R.A., Adibhatla, R.M., Hatcher, J.F., Franklin, J.L., 2002. Loss of cardiolipin and mitochondria during programmed neuronal death: evidence of a role for lipid peroxidation and autophagy. Neuroscience 115 (2), 587–602.

Kissova, I., Deffieu, M., Manon, S., Camougrand, N., 2004. Uth1p is involved in the autophagic degradation of mitochondria. J. Biol. Chem. 279 (37), 39068–39074.

Morita, E., Sugamura, K., 2002. Human parvovirus B19-induced cell cycle arrest and apoptosis. Springer Semin. Immunopathol. 24 (2), 187–199.

Morita, E., Tada, K., Chisaka, H., Asao, H., Sato, H., Yaegashi, N., Sugamura, K., 2001. Human parvovirus B19 induces cell cycle arrest at G (2) phase with accumulation of mitotic cyclins. J. Virol. 75 (16), 7555–7563.

Morita, E., Nakashima, A., Asao, H., Sato, H., Sugamura, K., 2003. Human parvovirus B19 nonstructural protein (NS1) induces cell cycle arrest at G (1) phase. J. Virol. 77 (5), 2915–2921.

Nakagawa, I., Amano, A., Mizushima, N., Yamamoto, A., Yamaguchi, H., Kamimoto, T., Nara, A., Funao, J., Nakata, M., Tsuda, K., Hamada, S., Yoshimori, T., 2004. Autophagy defends cells against invading group A Streptococcus. Science 306 (5698), 1037–1040.

Nakashima, A., Morita, E., Saito, S., Sugamura, K., 2004. Human Parvovirus B19 nonstructural protein transactivates the p21/WAF1 through Sp1. Virology 329 (2), 493–504.

Ozawa, K., Kurtzman, G., Young, N., 1987. Productive infection by B19 parvovirus of human erythroid bone marrow cells in vitro. Blood 70 (2), 384–391.

Tolkovsky, A.M., Xue, L., Fletcher, G.C., Borutaite, V., 2002. Mitochondrial disappearance from cells: a clue to the role of autophagy in programmed cell death and disease? Biochimie 84 (2–3), 233–240.

Yaegashi, N., Niinuma, T., Chisaka, H., Uehara, S., Moffatt, S., Tada, K., Iwabuchi, M., Matsunaga, Y., Nakayama, M., Yutani, C., Osamura, Y., Hirayama, E., Okamura, K., Sugamura, K., Yajima, A., 1999. Parvovirus B19 infection induces apoptosis of erythroid cells in vitro and in vivo. J. Infect. 39 (1), 68–76.

Yoshimori, T., 2004. Autophagy: a regulated bulk degradation process inside cells. Biochem. Biophys. Res. Commun. 313 (2), 453–458.

Young, N., Harrison, M., Moore, J., Mortimer, P., Humphries, R.K., 1984. Direct demonstration of the human parvovirus in erythroid progenitor cells infected in vitro. J. Clin. Invest. 74 (6), 2024–2032.

Yu, L., Alva, A., Su, H., Dutt, P., Freundt, E., Welsh, S., Baehrecke, E.H., Lenardo, M.J., 2004. Regulation of an ATG7-beclin 1 program of autophagic cell death by caspase-8. Science 304 (5676), 1500–1502.

Grb2 and Gads Exhibit Different Interactions with CD28 and Play Distinct Roles in CD28-Mediated Costimulation[1]

Ryosuke Watanabe,[2]* Yohsuke Harada,[2]* Kei Takeda,[2]* Jun Takahashi,* Kazunobu Ohnuki,* Shuhei Ogawa,* Daisuke Ohgai,* Nanako Kaibara,* Osamu Koiwai,[‡] Kazunari Tanabe,[§] Hiroshi Toma,[§] Kazuo Sugamura,[¶] and Ryo Abe[3]*[†]

Although both CD28 and ICOS bind PI3K and provide stimulatory signal for T cell activation, unlike CD28, ICOS does not costimulate IL-2 secretion. CD28 binds both PI3K and Grb2, whereas ICOS binds only PI3K. We have generated an ICOS mutant, which can bind Grb2 by replacement of its PI3K binding motif YMFM with the CD28 YMNM motif, and shown that it induces significant activation of the IL-2 promoter. However, this mutant ICOS was insufficient to activate the NF-κB pathway. In this study, we show that Gads, but not Grb2, is essential for CD28-mediated NF-κB activation, and its binding to CD28 requires the whole CD28 cytoplasmic domain in addition to the YMNM motif. Mutagenesis experiments have indicated that mutations in the N-terminal and/or C-terminal PXXP motif(s) of CD28 significantly reduce their association with Gads, whereas their associations with Grb2 are maintained. They induced strong activity of the NFAT/AP-1 reporter comparable with the CD28 wild type, but weak activity of the NF-κB reporter. Grb2- and Gads-dominant-negative mutants had a strong effect on NFAT/AP-1 reporter, but only Gads-dominant-negative significantly inhibited NF-κB reporter. Our data suggest that, in addition to the PI3K binding motif, the PXXP motif in the CD28 cytoplasmic domain may also define a functional difference between the CD28- and ICOS-mediated costimulatory signals by binding to Gads. *The Journal of Immunology,* **2006, 177: 1085–1091.**

Ligation of TCRs alone is insufficient to induce full activation of T lymphocytes. Additional ligand-receptor interactions on APCs and T cells are required. The best characterized costimulatory pair is CD28 and its ligands, CD80 (B7-1) and CD86 (B7-2) (1, 2). CD28 provides a costimulatory signal that is required for full T cell activation and expression of T cell functions. Although many studies have demonstrated the importance of CD28 costimulation in T cell function, the molecular mechanism underlying intracellular signal transduction triggered by CD28 ligation is poorly understood. It has been reported that CD28 associates with signaling proteins such as PI3K, Grb2 family adaptor proteins, Grb2 and Gads/Grf40, Tec family protein tyrosine kinases, Itk and Tec, and Lck (2–4). Among them, PI3K, Grb2, and Gads bind to the YMNM motif in the CD28 cytoplasmic domain. However, the role of this YMNM motif in CD28-dependent costimulation is a matter of controversy. We have previously shown, using a transgenic approach, that the YMNM motif is critical for IL-2 production and that a single alteration of Y to F attenuates the normal in vivo expansion of alloreactive T cells in acute graft vs host disease (5). In contrast, other studies have shown that mutation of the tyrosine residue in the YMNM motif has little, if any, effect on proliferation and IL-2 production (6–8).

CD28 costimulation induces high levels of IL-2 production in T cells, whereas ICOS, which is the third member of the CD28 family of molecules, does not costimulate IL-2 production (9, 10). ICOS possesses an YMFM motif in a region corresponding to the CD28 YMNM motif. The single amino acid alteration in the ICOS YMFM motif allows ICOS to bind to PI3K but not to Grb2 (11, 12). Using CD28 YMNM point and deletion mutants, we have previously shown that the N191A mutant, which retains PI3K binding but loses Grb-2 binding, loses all IL-2 promoter activity (13). This finding prompted us to hypothesize that ICOS cannot induce IL-2 production, because it possesses the Grb-2 nonbinding YMFM motif instead of the YMNM motif in CD28. In fact, we found that the ICOS mutant, whose PI3K binding motif, YMFM, was replaced by the YMNM used in CD28, showed a significant ability for IL-2 promoter activation (11). Interestingly, we also observed that this mutant could fully activate the NFAT/AP-1 site in the IL-2 promoter, but not the CD28RE/AP-1 and NF-κB sites. These findings indicate that the difference of a single amino acid, which affects Grb2 binding ability, may define a functional difference between the CD28- and ICOS-mediated costimulatory signals, and that one or more CD28 binding molecules other than Grb2 and PI3K are required for full activation of the NF-κB pathway by CD28.

Grb2, which is an adaptor protein composed of two Src homology 3 (SH3)[4] domains and an intervening Src homology 2 (SH2) domain, is ubiquitously expressed. Grb2 plays a critical role in the regulation of Ras by interacting with son of sevenless, a guanine nucleotide exchange factor (14, 15). Gads, which is composed of two SH3 domains, an intervening SH2 domain and a unique insert

*Research Institute for Biological Sciences, [†]Genome and Drug Research Center, and [‡]Department of Applied Biological Science, Faculty of Science and Technology, Tokyo University of Science, Chiba, Japan; [§]Department of Urology, Tokyo Women's Medical University, Tokyo, Japan; and [¶]Department of Microbiology and Immunology, Tohoku University School of Medicine, Sendai, Japan

Received for publication August 30, 2004. Accepted for publication May 1, 2006.

The costs of publication of this article were defrayed in part by the payment of page charges. This article must therefore be hereby marked *advertisement* in accordance with 18 U.S.C. Section 1734 solely to indicate this fact.

[1] This work supported by a grant-in-aid for Scientific Research from the Ministry of Education, Science, Sports, and Culture, Japan.

[2] R.W., Y.H., and K.T. contributed equally to this work.

[3] Address correspondence and reprint requests to Dr. Ryo Abe, Research Institute for Biological Sciences, Tokyo University of Science, 2669 Yamazaki, Noda, Chiba 278-0022, Japan. E-mail address: rabe@rs.noda.tus.ac.jp

[4] Abbreviations used in this paper: SH3, Src homology 3; SH2, Src homology 2; SLP-76, SH2 domain-containing leukocyte protein of 76 kDa; PVDF, polyvinylidene difluoride; WT, wild type; DN, dominant negative; PKCθ, protein kinase Cθ.

0022-1767/06/$02.00

region containing proline/glutamine-rich sequence, is predominantly expressed in lymphoid tissue and hemopoietic cells, particularly in T cells (16–18). Gads associates constitutively with SH2 domain-containing leukocyte protein of 76 kDa (SLP-76), is recruited to linker for activation of T cells upon TCR ligation, and plays a major role in TCR signaling (18–21). Although the roles of these two Grb2 family molecules in TCR-mediated signaling have been well documented, their roles in CD28-mediated costimulation are yet to be defined. Using a CD28 mutant that is unable to bind Grb2, we and others have demonstrated that Grb2 and Gads are involved in CD28-mediated IL-2 production (13, 22, 23). However, this approach could not discriminate functional differences between Grb2 and Gads. In this report, we show that Gads is more efficiently involved in CD28-mediated *IL-2* gene transcription than Grb2, and suggest that maximal IL-2 promoter activation by CD28 ligation may primarily require activation of NF-κB by Gads.

Materials and Methods

Plasmids

Mutant CD28 and ICOS constructs were generated by oligonucleotide-directed site-specific mutagenesis and verified by DNA sequencing. CD28 wild type (WT), ICOS WT, and their mutant constructs were subcloned into the mammalian expression vector pcDNA3.1/Zeo (Invitrogen Life Technologies) and a pMX-GFP vector (24). The CD28RE/AP-1 Luc reporter construct was obtained from A. Weiss (University of California, San Francisco, CA). The IL-2, NFAT/AP-1, AP-1, and NF-κB Luc reporter constructs were obtained from K. Arai (University of Tokyo, Tokyo, Japan). pcDNA-Myc-Gads-dSH2 and pcDNA-Myc-Grb2-dSH2 were described previously (18).

GST-fusion proteins

The cDNA encoding the cytoplasmic domain of CD28 or ICOS was amplified by PCR and cloned into the pGEX4T-1 vector (Amersham Biosciences). Tyrosine-nonphosphorylated GST-CD28 and GST-ICOS were expressed in the *Escherichia coli* BL21 (DE3) strain (Novagen). Tyrosine-phosphorylated GST-CD28 and GST-ICOS were expressed in the *E. coli* TKB1 strain (Stratagene), a BL21 (DE3) derivative strain that harbors a plasmid-encoded, inducible tyrosine kinase gene. Bacterial cultures were grown to log phase, induced by 0.3 mM isopropyl-1-thio-β-D-galactopyranoside, and incubated 3 h at 37°C. The bacteria were lysed and purified on glutathione-Sepharose beads (Amersham Biosciences).

Immunoprecipitation, GST precipitation, and Western immunoblots

For immunoprecipitation, 2×10^7 cells were mixed with equal numbers of Ab-coated Sepharose-CL4B beads in the presence of 100 μM pervanadate for 30 min at 37°C. After washing twice with cold PBS, cells and beads were resuspended in lysis buffer (50 mM Tris (pH 7.4), 1% Nonidet P-40, 0.25% Na-deoxycholate, 150 mM NaCl, 1 mM EGTA, 1 mM PMSF, 1 mM Na_3VO_4, 1 mM NaF) and incubated for 1 h at 4°C. The beads were pelleted and washed three times in cold lysis buffer. Proteins were eluted by boiling for 10 min in SDS lysis buffer and were separated by SDS-PAGE. For GST precipitation, Jurkat cells were lysed in the lysis buffer (1% Nonidet P-40, 20 mM Tris (pH 7.5), 150 mM NaCl, 5 mM EDTA, 10 μg/ml leupeptin, 10 μg/ml aprotinin, 1 mM Na_3VO_4, and 50 mM NaF). The lysates was centrifuged at 20,000 × *g* for 10 min, and the supernatant was incubated with immobilized GST-fusion proteins on glutathione beads for 2 h at 4 °C. The beads were washed three times with lysis buffer and boiled in the presence of SDS sample buffer. The protein complexes were resolved by SDS-PAGE (12.5%) and transferred to polyvinylidene difluoride (PVDF) membranes, and immunoblotted with antiserum specific for the p85 subunit of PI3K (Upstate Biotechnology) or antiserum specific for Gads (18), or anti-Grb2 Ab (C-23; Santa Cruz Biotechnology).

Cell culture, transfections, and retrovirus infection

Jurkat-TAg cells were maintained in RPMI 1640 supplemented with 10% FCS, penicillin, streptomycin, 10 mM HEPES (pH 7.55), and 50 μM 2-ME. For transient transfections, exponentially growing cells were harvested, washed in PBS, and resuspended at 4×10^7 cells/ml. A total of 1×10^7 cells (0.25 ml) was combined 5 μg of effector construct and 5 μg of the luciferase reporter gene in a 4-mm cuvette and electroporated with a Bio-Rad Gene Pulser at 240 V and 950 μF (Bio-Rad Laboratories). For retrovirus infection, plasmids were transfected into a packaging cell line, PLAT-E (25), using FuGENE6 (Roche), and, after incubation for 24 h, the culture supernatant was harvested and used as a viral stock. Ecotropic viral receptor expressing Jurkat (J.EcoR) cells (26) were infected with retrovirus by incubating with 1 ml of viral stock for 2 days.

Reporter assay

Jurkat-TAg cells were transiently cotransfected with effecter and reporter constructs together with pSV2A-PAP. The PAP plasmid was used for normalizing the transfection efficiency. After 24 h, cells were treated with PMA (5 ng/ml; LC Services) and anti-mouse CD28 mAb PV-1 (5 μg/ml) (13). After 8 h, cell lysates were analyzed for luciferase activity using a luciferase assay kit (Promega). Briefly, cells were resuspended in 100 μl of lysis buffer and incubated at room temperature for 15 min. After a brief centrifugation, 50 μl of the supernatant was used with 100 μl of luciferase assay reagent. Luminescence was measured immediately with a Lumat LB9501 (Berthold).

Results

Gads, but not Grb2, binding to CD28 requires the CD28 cytoplasmic domain outside of the YMNM motif

CD28 costimulation induces high levels of IL-2 production in T cells, whereas ICOS does not costimulate IL-2 production. ICOS possesses an YMFM motif in the region corresponding to the CD28 YMNM motif (Fig. 1). This single amino acid alteration results in the ICOS YMFM motif binding to PI3K but not to Grb2 (11, 12). Using CD28 mutants that selectively bind to PI3K or Grb2, we have previously shown that Grb2 but not PI3K has a stimulatory role in CD28-mediated IL-2 promoter activation (13). Furthermore, we found that a mutant ICOS that contains the CD28 YMNM motif and thus can bind to both PI3K and Grb2 induces substantial activation of the IL-2 promoter compared with ICOS WT (11). CD28 costimulation contributes to activation of the IL-2 promoter by up-regulating the activity of several transcription factors, so we used reporter constructs that contained the NFAT/AP-1 or NF-κB site to dissect the effect of Grb-2 binding to ICOS. Jurkat cells were transfected with ICOS WT, ICOS YMNM, or an ICOS-CD28 chimera, which contains the extracellular and transmembrane domains of ICOS fused to the cytoplasmic region of CD28, together with NFAT/AP-1 or NF-κB reporter plasmids. Promoter activation by PMA and anti-ICOS Abs was measured. As shown in Fig. 2, *A* and *B*, the ICOS-CD28 chimera, but not ICOS WT, induced marked activation of the NFAT/AP-1 and NF-κB reporters. Interestingly, it was found that the ICOS YMNM mutant induced strong activity of the NFAT/AP-1 reporter comparable with the ICOS-CD28 chimera, whereas it induced very weak activity of the NF-κB reporter. These findings indicate that the binding of Grb2 and PI3K is not sufficient for activation of the NF-κB pathway by CD28. In addition to Grb2, another Grb2 family molecule, Gads, is known to bind to CD28. Therefore, we examined whether the ICOS YMNM mutant has the same ability to bind to Gads as CD28. As shown previously, the ICOS WT associated with PI3K, but not with Grb2, in a phosphorylation-dependent manner. The ICOS YMNM mutant had binding affinities for both PI3K and

CD28 WT	IWTNSRRNRLLQSDYMNMTPRRPGLTRKPYQPYAPARDFAAYRP
CD28 nPA	IWTNSRRNRLLQSDYMNMTARRAGLTRKPYQPYAPARDFAAYRP
CD28 cPA	IWTNSRRNRLLQSDYMNMTPRRPGLTRKPYQAYAAARDFAAYRP
CD28 ncPA	IWTNSRRNRLLQSDYMNMTARRAGLTRKPYQAYAAARDFAAYRP
ICOS WT	KKKYGSSVHDPNSEYMFMAAVNTNKKSRLAGVTS
ICOS YMNM	KKKYGSSVHDPNSEYMNMAAVNTNKKSRLAGVTS

FIGURE 1. Cytoplasmic region amino acid sequences of the CD28, ICOS, and their mutants. The PI3K binding motif in CD28 and ICOS sequences, and PXXP motifs present in CD28 sequence are boxed. Mutations introduced for this study are indicated by underlining.

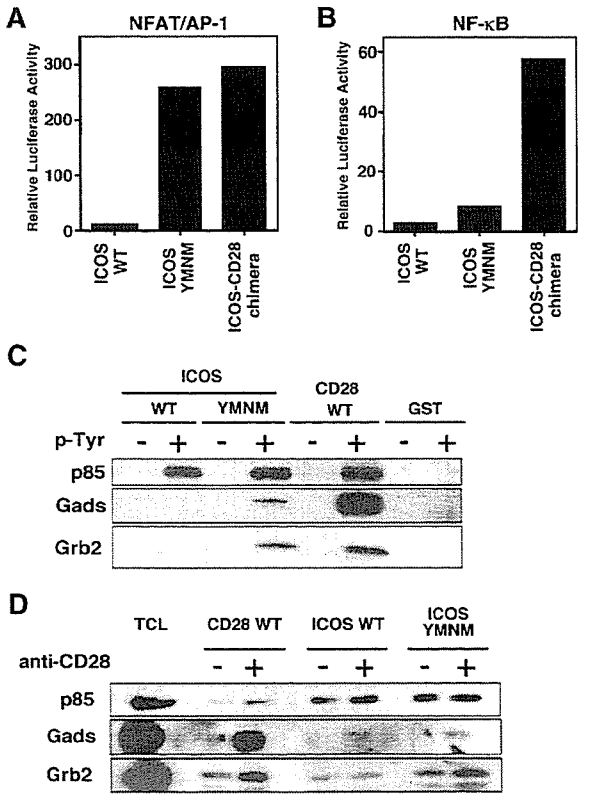

FIGURE 2. CD28 cytoplasmic domain outside of the YMNM motif plays an important role for NF-κB activation as well as Gads binding to CD28. *A* and *B*, CD28 cytoplasmic domain outside of the YMNM motif is required for NF-κB, but not NFAT activation. Mouse ICOS-WT, -YMNM mutant, or -CD28 chimera were transiently cotransfected with the NFAT/AP-1 (*A*)- or NF-κB (*B*)-reporter gene in 1×10^7 Jurkat-TAg cells (20 μg/ml) as described in *Materials and Methods*. Twenty-four hours after transfection, these cells were treated with PMA (5 ng/ml) and anti-ICOS Ab (5 μg/ml). Eight hours later, cells were lysed, and luciferase activity in the cell lysate was measured. All results shown are representative of at least three independent experiments. *C*, Whole CD28 molecule is required high-affinity binding of Gads to CD28. Jurkat cell lysates were incubated with immobilized GST, GST-ICOS, GST-ICOS YMNM mutant, or GST-CD28. Precipitates were subjected to SDS-PAGE and immunoblotted with anti-p85 antiserum (*upper panel*), anti-Gads Ab (*middle panel*), and anti-Grb2 Ab (*lower panel*). *D*, In vivo interaction of CD28 with PI3K, Gads, and Grb-2. Jurkat cells that stably expressed CD28 WT, CD28-ICOS chimera, and CD28-ICOS YMNM mutant were incubated with anti-CD28 Ab-coated Sepharose-CL4B beads in the presence of 100 μM pervanadate for 30 min at 37°C before immunoprecipitation. The cells were lysed in lysis buffer, and then the beads were pelleted. The protein complexes were eluted by boiling for 10 min in SDS lysis buffer, separated by SDS-PAGE, transferred to PVDF membranes, and immunoblotted with anti-p85 antiserum (*upper panel*), anti-Grb2 Ab (*middle panel*), and anti-Gads Ab (*lower panel*).

Grb2 that were comparable with those of CD28. However, the ICOS YMNM mutant showed very weak binding to Gads compared with CD28 (Fig. 2*C*). These results indicate that Gads but not Grb2 binding to CD28 requires the CD28 cytoplasmic domain not just the YMNM motif. It should be noted that there is significant association of Gads with WT CD28 comparable with Grb2 association.

Next, we have examined, using immunoprecipitation experiments, the in vivo interactions between the intracellular portion of CD28, ICOS, and the ICOS-YMNM mutant and PI3K, Grb2, and Gads. Because the ICOS-specific mAb that we used failed to efficiently immunoprecipitate the target molecule, we generated Jurkat cells that stably expressed CD28 WT, the CD28-ICOS chimera, and the CD28-ICOS YMNM mutant at similar levels, as confirmed by flow cytometry analysis (data not shown). These cells were stimulated with anti-CD28 mAb and their lysates were immunoprecipitated and examined for associated PI3K, Grb2, and Gads by immunoblotting with their specific Abs. As shown in Fig 2*D*, PI3K, Grb2, and Gads all coprecipitated with CD28 WT after CD28 ligation. Significant association of Grb2 with CD28 WT and its mutants was observed in unstimulated Jurkat cells. In contrast, the cytoplasmic portion of ICOS WT showed no significant binding to Gads as well as no enhancement of Grb2 binding by receptor ligation, whereas ICOS-YMNM did significantly enhance binding to both Gads and Grb2 by receptor ligation. Consistent with the pull-down experiments shown in Fig 2*C*, the association of Gads with CD28 WT was much stronger than that with ICOS-YMNM. These results indicate that the YMNM motif is critical for receptor ligation-dependent binding of both Grb2 family molecules, and that the association between Gads and CD28 requires the cytoplasmic portion in addition to the YMNM motif.

Gads is involved in CD28-mediated IL-2 promoter activation more effectively than Grb2

The above results prompted us to hypothesize that the inability of the ICOS YMNM mutant to activate NF-κB could be due to the poor ability of this mutant to bind to Gads and that Gads binding to CD28 may have a critical role in NF-κB activation by CD28.

To elucidate the role of Grb2 and Gads in CD28-mediated costimulation, Jurkat cells were transiently transfected with Gads and Grb2 mutant plasmids lacking the SH2 domain (Gads-dominant-negative (DN) and Grb2-DN, respectively) or with vector alone (mock), along with an IL-2 promoter reporter and mouse CD28 construct. Expression of CD28 was measured by FACS (Fig. 3*A*) and that of Gads-DN and Grb2-DN was tested by immunoblotting with anti-Myc mAb (*B*). As shown in Fig. 3*A*, CD28 expression was almost equal among mock-, Gads-DN-, and Grb2-DN-transfected cells (*A*), and the expression of Gads-DN and Grb2-DN in each cell line was also similar (*B*). Under these conditions, the cell lines were stimulated with anti-CD28 mAb, and IL-2 promoter activation was measured. As shown in Fig. 3*C*, although both Gads-DN and Grb2-DN inhibited CD28-mediated IL-2 promoter activation, the suppressive effect of Gads-DN was significantly stronger than that of Grb2-DN. To confirm these results, both DN plasmids were transfected into Jurkat cells at various doses, and induction of their IL-2 promoter activation by CD28 stimulation was measured. As shown in Fig. 3*D*, for each dose of DN plasmid, Gads-DN showed a stronger inhibitory effect than Grb-2-DN. These results indicate that both Gads and Grb2 play stimulatory roles in CD28-mediated IL-2 promoter activation and that Gads is involved in CD28-mediated IL-2 promoter activation more effectively than Grb2.

Gads is involved in CD28-mediated NF-κB activation

The mechanism of *IL-2 gene* transcription in response to T cell activation has been well studied. The nature of IL-2 promoter activation seems to be the result of coordinate binding of many transcription factors to their recognition sequences on the promoter leading to the assembly of a functional unit (27, 28). Several studies have demonstrated a critical role of CD28 in facilitating maximal IL-2 promoter activation. CD28 induces maximal IL-2 promoter activation through the activation of the transcription factors, NFAT, AP-1, and the NF-κB/Rel family, particularly c-Rel (29–32). To test which transcription factors are activated downstream of Grb2 and Gads, Jurkat cells were transiently transfected with

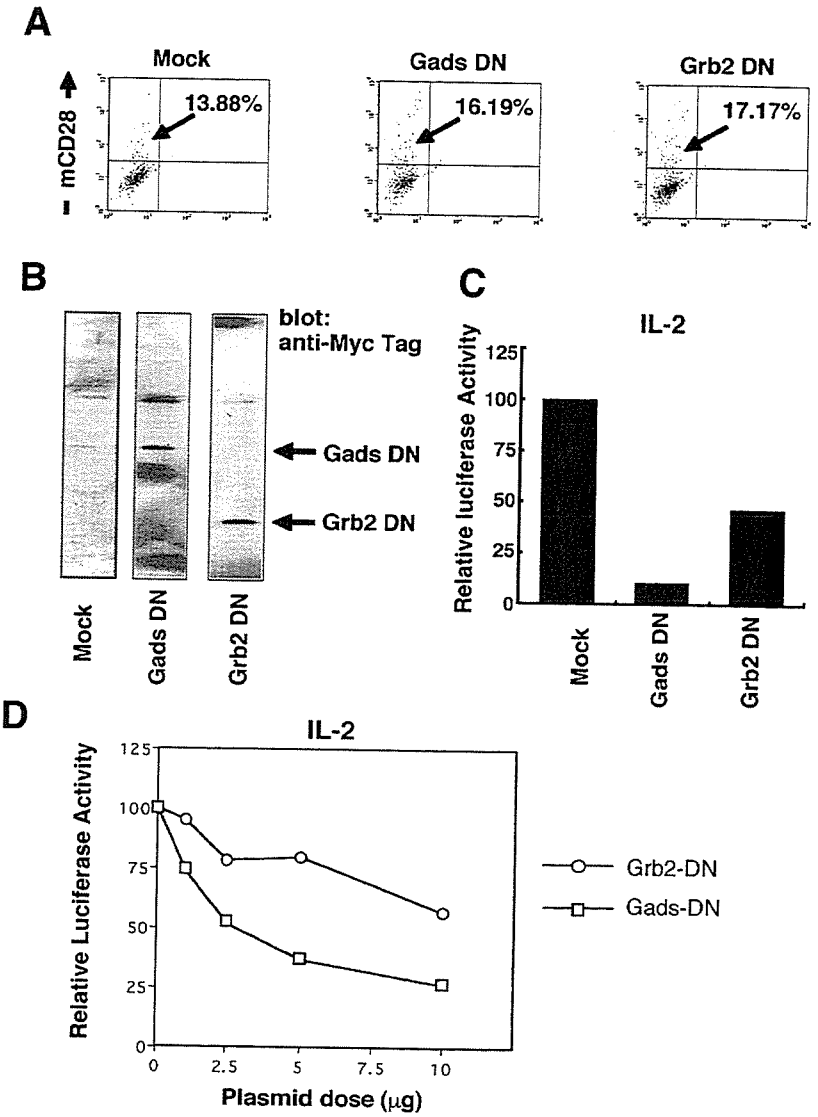

FIGURE 3. Gads is involved in CD28-mediated IL-2 promoter activation more effectively than Grb2. Jurkat-TAg cells were transiently cotransfected with murine CD28 WT and empty vector (mock), Myc-tagged Gads-DN, or Grb2-DN together with IL-2-Luc in 1×10^7 (20 μg/ml) as described in *Materials and Methods*. *A*, CD28 expression was almost equal among mock-, Gads-DN-, and Grb2-DN-transfected cells. Thirty-two hours after electroporation, Jurkat transfectants were analyzed by flow cytometry. *B*, The expression of Gads-DN and Grb2-DN. Thirty-two hours after electroporation, cells were lysed, separated by SDS-PAGE, transferred to PVDF membranes, and immunoblotted with anti-Myc Ab. *C*, The effect of Gads-DN and Grb2-DN in CD28-mediated IL-2 promoter activation. Twenty-four hours after electroporation, Jurkat transfectants were stimulated with PMA (5 ng/ml) and anti-CD28 Abs (5 μg/ml) for 8 h and assayed for luciferase activity. *D*, Gads is involved in CD28-mediated IL-2 promoter activation more effectively than Grb2. Jurkat cells were transiently transfected with the indicated doses of Gads-DN and Grb2-DN along with mouse CD28 and IL-2-Luc.

Gads- or Grb2-DN along with CD28RE/AP-1 (Fig. 4*A*), NFAT/AP-1 (*B*), AP-1 (*C*), or NF-κB (*D*)-dependent luciferase reporter constructs. Similar to their effects on the IL-2 promoter, Gads-DN inhibited PMA and anti-CD28-induced activation of CD28RE/AP-1, NFAT/AP-1, and AP-1 reporter more effectively than did Grb2-DN. Interestingly, Gads-DN could significantly inhibit PMA and anti-CD28-induced activation of the NF-κB reporter, whereas Grb2-DN failed to show an inhibitory effect. These data indicate that Gads's dominance over Grb2 in CD28-mediated IL-2 promoter activation most likely results from Gads's efficient activation of CD28RE/AP-1, NFAT/AP-1, and AP-1 and its independent activation of NF-κB.

Gads binding to CD28 correlates with NF-κB activation

It has been reported that association of Grb2 and Gads with CD28 is stabilized by interactions between the SH3 domain of Grb2 or Gads and the PXXP motif in the CD28 cytoplasmic domain (4, 23, 33). Because the ICOS YMNM mutant has no PXXP motif (Fig. 1*A*), we believed that the PXXP motif of CD28 may be more critical for Gads binding than for Grb2 binding. To test this hypothesis, we generated tyrosine-phosphorylated GST-CD28 fusion proteins carrying two proline-to-alanine mutations in the N-terminal PXXP motif (nPA mutant), in the C-terminal PXXP motif (cPA mutant), and in both PXXP motifs (ncPA mutant), and examined their ability to bind to PI3K p85, Grb2, and Gads (Fig. 5*A*). All CD28 fusion proteins bound equally to p85. The cPA mutant associated with Grb2 to a similar degree as CD28 WT, whereas binding of nPA and ncPA mutants to Grb2 was slightly weaker than WT. In contrast, the association of nPA and ncPA mutants with Gads was strongly reduced, and the association of cPA with Gads was also, albeit to a lesser extent, significantly weaker than the association of CD28 WT with Gads.

Next, we have examined, using immunoprecipitation experiments, the in vivo interactions between the intracellular portion of WT and mutant CD28, and PI3K, Grb2, and Gads. We generated Jurkat cells that stably expressed WT and proline mutants of mouse CD28. These cell lines express mouse CD28 at similar levels, as confirmed by flow cytometry analysis (data not shown). The cells were stimulated with anti-CD28 mAb, and their lysates were immunoprecipitated and examined for associated PI3K, Grb2, and Gads by immunoblotting with their specific Abs. As shown in Fig. 5*B*, similar to the results of pull-down assay, the association of nPA and ncPA mutants with Gads was strongly reduced, and the association of cPA with Gads was weakly, but consistently reduced. These results suggest that the PXXP motif in the CD28 cytoplasmic domain play a critical role in the association of Gads

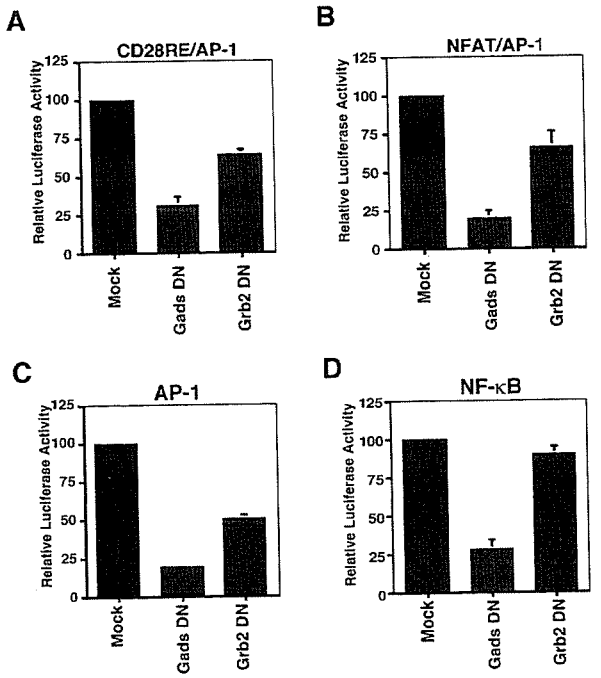

FIGURE 4. Gads is involved in CD28-mediated NF-κB activation. Jurkat-TAg cells were transiently cotransfected with murine CD28 WT and empty vector (mock), Gads-DN, or Grb2-DN together with CD28RE/AP-1 (*A*), NFAT/AP-1 (*B*), AP-1 (*C*), or NF-κB (*D*) reporter plasmids. Twenty-four hours later, the cells were stimulated with PMA (5 ng/ml) and anti-CD28 Abs (5 μg/ml) for 8 h and assayed for luciferase activity. Bars show the mean and SD of three representative experiments as a percentage of luciferase activity of mock transfectants.

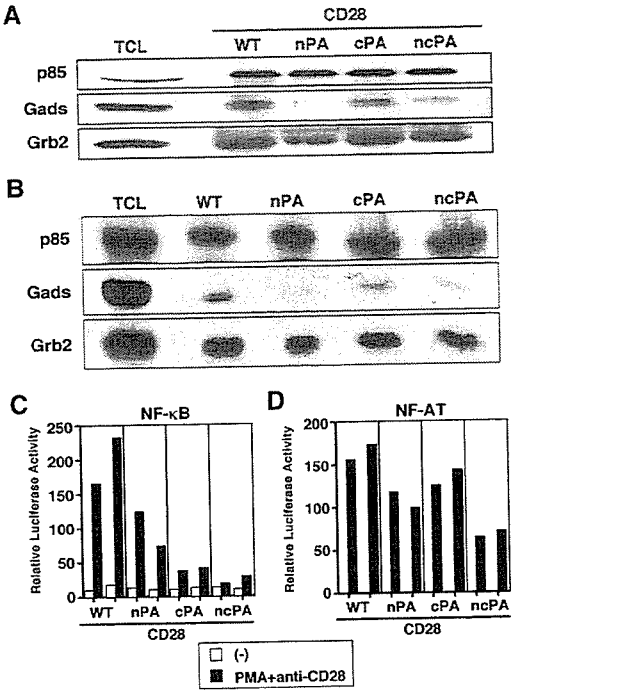

FIGURE 5. Gads binding to CD28 correlates with NF-κB reporter activation. *A*, Jurkat cell lysates were incubated with immobilized tyrosine-phosphorylated GST-normal CD28 fusion protein (WT) and GST-CD28 fusion protein carrying mutation of two prolines to alanines in N-terminal PXXP motif (nPA mutant), in C-terminal PXXP motif (cPA mutant), and in both PXXP motifs (ncPA mutant) for 2 h at 4°C. The beads were washed three times with lysis buffer and boiled in the presence of SDS sample buffer. The protein complexes were resolved by SDS-PAGE (12.5%) and transferred to PVDF membranes, and immunoblotted with Ab specific for the p85 subunit of PI3K, Gads, or Grb2 Ab. *B*, Jurkat cells that stably expressed CD28 WT, CD28 nPA, CD28 cPA, and CD28 ncPA mutant were incubated with anti-CD28 Ab-coated Sepharose-CL4B beads in the presence of 5 ng/ml PMA for 30 min at 37°C before immunoprecipitation. The cells were lysed in lysis buffer, and then the beads were pelleted. The protein complexes were eluted by boiling for 10 min in SDS lysis buffer, separated by SDS-PAGE, transferred to PVDF membranes, and immunoblotted with anti-p85 antiserum (*upper panel*), anti-Gads Ab (*middle panel*), and anti-Grb2 Ab (*lower panel*). *C* and *D*, Jurkat TAg cells were transiently transfected with NF-κB (*C*) or NFAT/AP-1 (*D*) reporter plasmids (20 μg/ml) along with CD28 mutants. Twenty-four hours later, the cells were stimulated with PMA (5 ng/ml) and anti-CD28 Abs (5 μg/ml) for 8 h and assayed for luciferase activity. These results are representative from at least three independent experiments.

with CD28. We then examined the function of PXXP in NF-κB and NFAT activation. Jurkat cells were transiently transfected with WT or PXXP mutants of CD28 along with NF-κB or NFAT/AP-1-dependent luciferase reporter constructs. Similar levels of expression of CD28 in the transfected cells were confirmed by FACS analysis (data not shown). As shown in Fig. 5*B*, NF-κB activation was strongly reduced in cells transfected with any of the PXXP mutants compared with those transfected with WT. Interestingly, unlike its effects on association (Fig. 5*A*), mutation of the C-terminal PXXP motif resulted in a stronger reduction in NF-κB activation than N-terminal PXXP. Compared with NF-κB, NFAT activation was much less influenced by the proline mutations (Fig. 5*C*). In particular, although mutation of both the N-terminal and C-terminal PXXP motifs significantly inhibited NFAT activation, mutation of either the N-terminal or C-terminal alone only showed slight inhibition. These results indicate that the association of Gads with CD28 through Gads-SH3 and CD28 PXXP motifs requires CD28 costimulation-dependent NF-κB activation.

Discussion

Although the roles and functions of Gads and Grb2 in TCR-mediated signaling are well characterized and documented, their roles in CD28-mediated signaling remain unknown. Using a CD28 mutant that is unable to bind Grb2, we and others (13, 22, 23) have demonstrated that Grb2 and Gads are involved in CD28-mediated IL-2 production. However, this approach could not discriminate functional differences between Grb2 and Gads. In this report, we have found that molecules belonging to the Grb2 family play a critical role in CD28-mediated IL-2 promoter activation and that, of these, Gads plays a dominant role in CD28-mediated IL-2 promoter activation (Fig. 3). Asada et al. (18) have shown that overexpression of Gads-DN results in dominant inhibition of TCR-induced IL-2 promoter activation compared with Grb2-DN. These results suggest that Gads has a more important role in both TCR- and CD28-mediated signal transduction pathways than Grb2. Because Gads shows greater binding affinity to SLP-76 compared with Grb2, it is conceivable that Gads plays a key role in bringing SLP-76 to membrane-bound linker for activation of T cells during TCR signaling (18–21). We observed that CD28 associated with SLP-76 via Gads in HEK 293T cells (data not shown). CD28 may also recruit SLP-76 and its associated molecules such as Vav by binding to Gads. Furthermore, $p62^{dok}$ and receptor for activated C kinase-1 were found to associate with Gads but not with Grb2 (4). These molecules may determine functional differences between Gads and Grb2 in CD28 signaling.

We have demonstrated that the YMNM motif has a critical role in CD28-mediated costimulation in vitro and in vivo (5, 13). In

contrast, Okkenhaug et al. (6) showed that the mutant CD28 transgene in CD28-deficient mice had no effect on T cell proliferation and IL-2 production. Using a retroviral expression system, another study showed that mutation of the tyrosine residue in the YMNM motif only marginally reduced proliferation and IL-2 production (7). However, because their studies used TCR transgenic models in which the TCRs had high affinity for peptide Ags, the role of the YMNM motif may be underestimated. The YMNM motif might be more critical for CD28-mediated costimulation of T cell responses to low-affinity Ags such as in alloreaction than to high-affinity Ags. Moreover, by comparing CD28 with an ICOS YMNM mutant, we have also shown that the CD28 cytoplasmic domain outside of the YMNM motif is critical for CD28-mediated costimulation, especially for NF-κB activation (Fig. 2) (11). However, which CD28 binding molecule(s) are involved in CD28-mediated NF-κB activation is yet to be defined. In this report, we have shown that Gads binding to CD28 requires the other parts of the CD28 cytoplasmic domain not just the YMNM motif and is essential for CD28-mediated NF-κB activation. Although both molecules have two SH3 domains, our results suggest that the interaction between the YMNM motif and the SH2 domain is sufficient for Grb2 binding, whereas additional interactions between the PXXP motif and the SH3 domain are required for Gads binding. Consistent with this hypothesis, we observed that mutation of the PXXP motif has minimal effects on the affinity of CD28 for Grb2, whereas it dramatically reduced the affinity for Gads (Fig. 5*A*). Of the two PXXP motifs in CD28, mutation of the N-terminal PXXP resulted in a stronger reduction in Gads binding, suggesting that N-terminal PXXP has a higher affinity to Gads-SH3 than C-terminal PXXP. It should be noted that mutation of the C-terminal PXXP motif caused a stronger reduction in NF-κB activation than resulted from mutation of the N-terminal PXXP motif, and indicates that the C-terminal PXXP motif plays a more important role. This apparent discrepancy between the binding pattern of Gads and NF-κB activation may indicate that there are other signaling molecule(s) that are important for NF-κB activation that bind to the C-terminal PXXP motif. In fact, it has been shown that Lck binds the C-terminal PXXP motif (34).

The weak effect of mutations in the N- or C-terminal PXXP alone on NFAT activation is consistent with the idea that the CD28 cytoplasmic portion other than the YMNM motif play a minimal role in NFAT activation (Figs. 2 and 5). We observed that mutation of both PXXP motifs significantly reduces NFAT activation. It is conceivable that this mutation may cause structural change to the cytoplasmic portion of CD28, resulting in inhibition of the signal transduction cascade for NFAT activation.

Although a signal that leads to NF-κB activation is required for T cell functions triggered by CD28 ligation, the components of the signaling pathway are still poorly defined. One of them is protein kinase Cθ (PKCθ), which mediates NF-κB activation by CD28 through IκB kinase β activation (35, 36). Recently, another component of the NF-κB signaling pathway has been identified: the Bcl10, a caspase recruitment domain-containing adaptor protein identified from the t(1;14) (p22;q32) breakpoint in MALT lymphomas (37). Bcl10$^{-/-}$ T cells have the same phenotype as PKC$\theta^{-/-}$ T cells (38). This suggests that Bcl10 and PKCθ act along the same pathway. CARD-containing MAGUK protein 1, a lymphocyte-specific member of the membrane-associated guanylate kinase family of scaffolding proteins, can cooperate with Bcl10 to induce NF-κB activation (39–41). MALT1 also synergistically induces NF-κB activation with Bcl10 (42). It is conceivable that Gads plays a critical role in CD28-mediated NF-κB activation by cooperating with PKCθ, CARD-containing MAGUK protein 1, Bcl10, and MALT1. However, the signaling molecules linking Gads to these proteins have not been identified. It was reported that CD28 could cooperate with SLP-76 and VAV to up-regulate *IL-2* gene transcription independently of TCR ligation (31). In addition, VAV has been reported to promote PKCθ translocation from the cytosol to the membrane and cytoskeleton and to induce its enzymatic activation (43). Gads may recruit the SLP-76-VAV complex to the CD28 cytoplasmic domain and activate the PKCθ-IκB kinase pathway leading to the activation of NF-κB. Further studies will be required to determine what molecules mediate the interaction between Gads and NF-κB.

It has been reported that ICOS performs distinct costimulatory functions from CD28 in various immune responses (12, 44, 45). This functional difference between CD28- and ICOS-mediated costimulation appears to be caused by their different cytokine production capabilities. Although both CD28- and ICOS-mediated costimulation affects the majority of cytokines produced, the ICOS-mediated signal does not enhance IL-2 production. ICOS possesses an YMFM motif in the region corresponding to the CD28 YMNM motif. We have previously suggested that this single amino acid alteration, which affects Grb2 binding ability, may be responsible for a functional difference between CD28 and ICOS. Recently Parry et al. (46) showed, using lentiviral expression systems to express mutant CD28 in primary human CD4$^+$ T cells, that even though the ICOS SH2 binding domain strongly activates PI3K, it is unable to act as a substitute for the CD28 SH2 binding domain to induce high levels of IL-2 and Bcl-x_L. Furthermore, the CD28 SH2 binding domain alone was sufficient to mediate optimal levels of Bcl-x_L induction, whereas the entire CD28 cytoplasmic tail was required for high levels of IL-2 expression.

Our data suggest that, in addition to a single amino acid alteration in the YMNM motif, the PXXP motif in the CD28 cytoplasmic domain, which is critical for Gads binding ability, may also define a functional difference between the CD28- and ICOS-mediated costimulatory signals.

Acknowledgments

We thank Dr. C. H. June and Dr. H. Kishimoto for helpful discussion and Dr. T. Kitamura and Dr. T. Saito for providing the pMX-GFP vector, PLAT-E cell, and J.EcoR cell. We also thank S. Watanabe for her secretarial assistance. We gratefully acknowledge a member of Science Service, Inc., for care of experimental animals.

Disclosures

The authors have no financial conflict of interest.

References

1. Jenkins, M. K., J. D. Ashwell, and R. H. Schwartz. 1988. Allogeneic non-T spleen cells restore the responsiveness of normal T cell clones stimulated with antigen and chemically modified antigen- presenting cells. *J. Immunol.* 140: 3324–3330.
2. Rudd, C. E., and H. Schneider. 2003. Unifying concepts in CD28, ICOS and CTLA4 co-receptor signalling. *Nat. Rev. Immunol.* 3: 544–556.
3. Schneider, H., Y. C. Cai, K. V. Prasad, S. E. Shoelson, and C. E. Rudd. 1995. T cell antigen CD28 binds to the GRB-2/SOS complex, regulators of p21^{ras}. *Eur. J. Immunol.* 25: 1044–1050.
4. Ellis, J. H., C. Ashman, M. N. Burden, K. E. Kilpatrick, M. A. Morse, and P. A. Hamblin. 2000. GRID: a novel grb-2-related adapter protein that interacts with the activated T cell costimulatory receptor CD28. *J. Immunol.* 164: 5805–5814.
5. Harada, Y., M. Tokushima, Y. Matsumoto, S. Ogawa, M. Otsuka, K. Hayashi, B. D. Weiss, C. H. June, and R. Abe. 2001. Critical requirement for the membrane-proximal cytosolic tyrosine residue for CD28-mediated costimulation in vivo. *J. Immunol.* 166: 3797–3803.
6. Okkenhaug, K., L. Wu, K. M. Garza, J. La Rose, W. Khoo, B. Odermatt, T. W. Mak, P. S. Ohashi, and R. Rottapel. 2001. A point mutation in CD28 distinguishes proliferative signals from survival signals. *Nat. Immunol.* 2: 325–332.
7. Burr, J. S., N. D. Savage, G. E. Messah, S. L. Kimzey, A. S. Shaw, R. H. Arch, and J. M. Green. 2001. Cutting edge: distinct motifs within CD28 regulate T cell proliferation and induction of Bcl-x_L. *J. Immunol.* 166: 5331–5335.
8. Andres, P. G., K. C. Howland, A. Nirula, L. P. Kane, L. Barron, D. Dresnek, A. Sadra, J. Imboden, A. Weiss, and A. K. Abbas. 2004. Distinct regions in the

CD28 cytoplasmic domain are required for T helper type 2 differentiation. *Nat. Immunol.* 5: 435–442.
9. Hutloff, A., A. M. Dittrich, K. C. Beier, B. Eljaschewitsch, R. Kraft, I. Anagnostopoulos, and R. A. Kroczek. 1999. ICOS is an inducible T-cell co-stimulator structurally and functionally related to CD28. *Nature* 397: 263–266.
10. Yoshinaga, S. K., J. S. Whoriskey, S. D. Khare, U. Sarmiento, J. Guo, T. Horan, G. Shih, M. Zhang, M. A. Coccia, T. Kohno, et al. 1999. T-cell co-stimulation through B7RP-1 and ICOS. *Nature* 402: 827–832.
11. Harada, Y., D. Ohgai, R. Watanabe, K. Okano, O. Koiwai, K. Tanabe, H. Toma, A. Altman, and R. Abe. 2003. A single amino acid alteration in cytoplasmic domain determines IL-2 promoter activation by ligation of CD28 but not inducible costimulator (ICOS). *J. Exp. Med.* 197: 257–262.
12. Coyle, A. J., S. Lehar, C. Lloyd, J. Tian, T. Delaney, S. Manning, T. Nguyen, T. Burwell, H. Schneider, J. A. Gonzalo, et al. 2000. The CD28-related molecule ICOS is required for effective T cell-dependent immune responses. *Immunity* 13: 95–105.
13. Harada, Y., E. Tanabe, R. Watanabe, B. D. Weiss, A. Matsumoto, H. Ariga, O. Koiwai, Y. Fukui, M. Kubo, C. H. June, and R. Abe. 2001. Novel role of PI3K in CD28-mediated costimulation. *J. Biol. Chem.* 276: 9003–9008.
14. Lowenstein, E. J., R. J. Daly, A. G. Batzer, W. Li, B. Margolis, R. Lammers, A. Ullrich, E. Y. Skolnik, D. Bar-Sagi, and J. Schlessinger. 1992. The SH2 and SH3 domain-containing protein GRB2 links receptor tyrosine kinases to ras signaling. *Cell* 70: 431–442.
15. Buday, L., S. E. Egan, P. Rodriguez Viciana, D. A. Cantrell, and J. Downward. 1994. A complex of Grb2 adaptor protein, Sos exchange factor, and a 36-kDa membrane-bound tyrosine phosphoprotein is implicated in ras activation in T cells. *J. Biol. Chem.* 269: 9019–9023.
16. Liu, S. K., and C. J. McGlade. 1998. Gads is a novel SH2 and SH3 domain-containing adaptor protein that binds to tyrosine-phosphorylated Shc. *Oncogene* 17: 3073–3082.
17. Law, C. L., M. K. Ewings, P. M. Chaudhary, S. A. Solow, T. J. Yun, A. J. Marshall, L. Hood, and E. A. Clark. 1999. GrpL, a Grb2-related adaptor protein, interacts with SLP-76 to regulate nuclear factor of activated T cell activation. *J. Exp. Med.* 189: 1243–1253.
18. Asada, H., N. Ishii, Y. Sasaki, K. Endo, H. Kasai, N. Tanaka, T. Takeshita, S. Tsuchiya, T. Konno, and K. Sugamura. 1999. Grf40, A novel Grb2 family member, is involved in T cell signaling through interaction with SLP-76 and LAT. *J. Exp. Med.* 189: 1383–1390.
19. Liu, S. K., N. Fang, G. A. Koretzky, and C. J. McGlade. 1999. The hematopoietic-specific adaptor protein gads functions in T-cell signaling via interactions with the SLP-76 and LAT adaptors. *Curr. Biol.* 9: 67–75.
20. Boerth, N. J., J. J. Sadler, D. E. Bauer, J. L. Clements, S. M. Gheith, and G. A. Koretzky. 2000. Recruitment of SLP-76 to the membrane and glycolipid-enriched membrane microdomains replaces the requirement for linker for activation of T cells in T cell receptor signaling. *J. Exp. Med.* 192: 1047–1058.
21. Yoder, J., C. Pham, Y. M. Iizuka, O. Kanagawa, S. K. Liu, J. McGlade, and A. M. Cheng. 2001. Requirement for the SLP-76 adaptor GADS in T cell development. *Science* 291: 1987–1991.
22. Crooks, M. E., D. R. Littman, R. H. Carter, D. T. Fearon, A. Weiss, and P. H. Stein. 1995. CD28-mediated costimulation in the absence of phosphatidylinositol 3-kinase association and activation. *Mol. Cell. Biol.* 15: 6820–6828.
23. Kim, H. H., M. Tharayil, and C. E. Rudd. 1998. Growth factor receptor-bound protein 2 SH2/SH3 domain binding to CD28 and its role in co-signaling. *J. Biol. Chem.* 273: 296–301.
24. Misawa, K., T. Nonaka, S. Morita, A. Kaneko, T. Nakahata, S. Asano, and T. Kitamura. 2000. A method to identify cDNAs based on localization of green fluorescent protein fusion products. *Proc. Natl. Acad. Sci. USA* 97: 3062–3066.
25. Morita, S., T. Kojima, and T. Kitamura. 2000. Plat-E: an efficient and stable system for transient packaging of retroviruses. *Gene Ther.* 7: 1063–1066.
26. Yamasaki, S., K. Nishida, M. Hibi, M. Sakuma, R. Shiina, A. Takeuchi, H. Ohnishi, T. Hirano, and T. Saito. 2001. Docking protein Gab2 is phosphorylated by ZAP-70 and negatively regulates T cell receptor signaling by recruitment of inhibitory molecules. *J. Biol. Chem.* 276: 45175–45183.
27. Garrity, P. A., D. Chen, E. V. Rothenberg, and B. J. Wold. 1994. Interleukin-2 transcription is regulated in vivo at the level of coordinated binding of both constitutive and regulated factors. *Mol. Cell. Biol.* 14: 2159–2169.
28. Rothenberg, E. V., and S. B. Ward. 1996. A dynamic assembly of diverse transcription factors integrates activation and cell-type information for interleukin 2 gene regulation. *Proc. Natl. Acad. Sci. USA* 93: 9358–9365.
29. McGuire, K. L., and M. Iacobelli. 1997. Involvement of Rel, Fos, and Jun proteins in binding activity to the IL-2 promoter CD28 response element/AP-1 sequence in human T cells. *J. Immunol.* 159: 1319–1327.
30. Michel, F., G. Mangino, G. Attal-Bonnefoy, L. Tuosto, A. Alcover, A. Roumier, D. Olive, and O. Acuto. 2000. CD28 utilizes Vav-1 to enhance TCR-proximal signaling and NF-AT activation. *J. Immunol.* 165: 3820–3829.
31. Raab, M., S. Pfister, and C. E. Rudd. 2001. CD28 signaling via VAV/SLP-76 adaptors: regulation of cytokine transcription independent of TCR ligation. *Immunity* 15: 921–933.
32. Ghosh, P., T. H. Tan, N. R. Rice, A. Sica, and H. A. Young. 1993. The interleukin 2 CD28-responsive complex contains at least three members of the NF-κB family: c-Rel, p50, and p65. *Proc. Natl. Acad. Sci. USA* 90: 1696–1700.
33. Okkenhaug, K., and R. Rottapel. 1998. Grb2 forms an inducible protein complex with CD28 through a Src homology 3 domain-proline interaction. *J. Biol. Chem.* 273: 21194–21202.
34. Holdorf, A. D., J. M. Green, S. D. Levin, M. F. Denny, D. B. Straus, V. Link, P. S. Changelian, P. M. Allen, and A. S. Shaw. 1999. Proline residues in CD28 and the Src homology (SH)3 domain of Lck are required for T cell costimulation. *J. Exp. Med.* 190: 375–384.
35. Isakov, N., and A. Altman. 2002. Protein kinase Cθ in T cell activation. *Annu. Rev. Immunol.* 20: 761–794.
36. Lin, X., A. O'Mahony, Y. Mu, R. Geleziunas, and W. C. Greene. 2000. Protein kinase C-θ participates in NF-κB activation induced by CD3-CD28 costimulation through selective activation of IκB kinase β. *Mol. Cell. Biol.* 20: 2933–2940.
37. Ruland, J., G. S. Duncan, A. Elia, I. del Barco Barrantes, L. Nguyen, S. Plyte, D. G. Millar, D. Bouchard, A. Wakeham, P. S. Ohashi, and T. W. Mak. 2001. Bcl10 is a positive regulator of antigen receptor-induced activation of NF-κB and neural tube closure. *Cell* 104: 33–42.
38. Sun, Z., C. W. Arendt, W. Ellmeier, E. M. Schaeffer, M. J. Sunshine, L. Gandhi, J. Annes, D. Petrzilka, A. Kupfer, P. L. Schwartzberg, and D. R. Littman. 2000. PKC-θ is required for TCR-induced NF-κB activation in mature but not immature T lymphocytes. *Nature* 404: 402–407.
39. Gaide, O., B. Favier, D. F. Legler, D. Bonnet, B. Brissoni, S. Valitutti, C. Bron, J. Tschopp, and M. Thome. 2002. CARMA1 is a critical lipid raft-associated regulator of TCR-induced NF-κB activation. *Nat. Immunol.* 3: 836–843.
40. Wang, D., Y. You, S. M. Case, L. M. McAllister-Lucas, L. Wang, P. S. DiStefano, G. Nunez, J. Bertin, and X. Lin. 2002. A requirement for CARMA1 in TCR-induced NF-κB activation. *Nat. Immunol.* 3: 830–835.
41. Pomerantz, J. L., E. M. Denny, and D. Baltimore. 2002. CARD11 mediates factor-specific activation of NF-κB by the T cell receptor complex. *EMBO J.* 21: 5184–5194.
42. Lucas, P. C., M. Yonezumi, N. Inohara, L. M. McAllister-Lucas, M. E. Abazeed, F. F. Chen, S. Yamaoka, M. Seto, and G. Nunez. 2001. Bcl10 and MALT1, independent targets of chromosomal translocation in malt lymphoma, cooperate in a novel NF-κB signaling pathway. *J. Biol. Chem.* 276: 19012–19019.
43. Villalba, M., N. Coudronniere, M. Deckert, E. Teixeiro, P. Mas, and A. Altman. 2000. A novel functional interaction between Vav and PKCθ is required for TCR-induced T cell activation. *Immunity* 12: 151–160.
44. Ogawa, S., G. Nagamatsu, M. Watanabe, S. Watanabe, T. Hayashi, S. Horita, K. Nitta, H. Nihei, K. Tezuka, and R. Abe. 2001. Opposing effects of anti-activation-inducible lymphocyte-immunomodulatory molecule/inducible costimulator antibody on the development of acute versus chronic graft-versus-host disease. *J. Immunol.* 167: 5741–5748.
45. McAdam, A. J., T. T. Chang, A. E. Lumelsky, E. A. Greenfield, V. A. Boussiotis, J. S. Duke-Cohan, T. Chernova, N. Malenkovich, C. Jabs, V. K. Kuchroo, et al. 2000. Mouse inducible costimulatory molecule (ICOS) expression is enhanced by CD28 costimulation and regulates differentiation of $CD4^+$ T cells. *J. Immunol.* 165: 5035–5040.
46. Parry, R. V., C. A. Rumbley, L. H. Vandenberghe, C. H. June, and J. L. Riley. 2003. CD28 and inducible costimulatory protein Src homology 2 binding domains show distinct regulation of phosphatidylinositol 3-kinase, Bcl-x_L, and IL-2 expression in primary human CD4 T lymphocytes. *J. Immunol.* 171: 166–174.

Prostaglandin D_2 Plays an Essential Role in Chronic Allergic Inflammation of the Skin via CRTH2 Receptor[1]

Takahiro Satoh,[2,3]* Rie Moroi,[2]* Kosuke Aritake,[†] Yoshihiro Urade,[†] Yasumasa Kanai,* Koji Sumi,* Hiroo Yokozeki,* Hiroyuki Hirai,[‡] Kinya Nagata,[‡] Toshifumi Hara,[§] Masanori Utsuyama,[¶] Katsuiku Hirokawa,[¶] Kazuo Sugamura,[‖] Kiyoshi Nishioka,* and Masataka Nakamura[§]

PGD_2 plays roles in allergic inflammation via specific receptors, the PGD receptor designated DP and CRTH2 (chemoattractant receptor homologous molecule expressed on Th2 cells). We generated mutant mice carrying a targeted disruption of the *CRTH2* gene to investigate the functional roles of CRTH2 in cutaneous inflammatory responses. CRTH2-deficent mice were fertile and grew normally. Ear-swelling responses induced by hapten-specific IgE were less pronounced in mutant mice, giving 35–55% of the responses of normal mice. Similar results were seen in mice treated with a hemopoietic PGD synthase inhibitor, HQL-79, or a CRTH2 antagonist, ramatroban. The reduction in cutaneous responses was associated with decreased infiltration of lymphocytes, eosinophils, and basophils and decreased production of macrophage-derived chemokine and RANTES at inflammatory sites. In models of chronic contact hypersensitivity induced by repeated hapten application, CRTH2 deficiency resulted in a reduction by approximately half of skin responses and low levels (63% of control) of serum IgE production, although in vivo migration of Langerhans cells and dendritic cells to regional lymph nodes was not impaired in CRTH2-deficient mice. In contrast, delayed-type hypersensitivity to SRBC and irritation dermatitis in mutant mice were the same as in wild-type mice. These findings indicate that the PGD_2-CRTH2 system plays a significant role in chronic allergic skin inflammation. CRTH2 may represent a novel therapeutic target for treatment of human allergic disorders, including atopic dermatitis. *The Journal of Immunology,* **2006, 177: 2621–2629.**

Prostaglandin D_2, a major product of cyclooxygenase in activated mast cells, exhibits a wide range of biological activities including vasodilatation, bronchoconstriction, and inhibition of platelet aggregation (1–4). High levels of PGD_2 are seen in bronchoalveolar lavage fluid during allergen-induced airway inflammation (5). Transgenic mice overexpressing lipocalin-type PGD synthase (PGDS)[4] demonstrate strong allergic lung responses and eosinophilia (6). Thus, PGD_2 has long been implicated in allergic diseases.

It is thought that PGD_2 exerts its physiological effects through the classical PGD receptor (DP), which is expressed in a variety of cell lineages (7). Signals from DP inhibit chemotaxis of eosinophils and dendritic cells (DC) in vitro (8, 9). Mice with targeted disruption of the *DP* gene exhibit reduced eosinophil infiltration into the lung and fail to develop airway hyperreactivity in response to allergen exposure (10). It is possible that DP-mediated signals are involved in allergic inflammation and, thus, another receptor for PGD_2 may be postulated. Indeed, we recently identified CRTH2 (chemoattractant receptor homologous molecule expressed on Th2 cells), which acts as a PGD_2 receptor with properties different from those of DP (11).

CRTH2 and DP are members of the G protein-coupled, seven-transmembrane receptor family. CRTH2 is coupled with G_i, whereas G_s is associated with DP (11). CRTH2 is expressed in eosinophils, basophils, and a subpopulation of Th2 cells and monocytes in humans (12). Upon treatment with PGD_2, these cells exhibit chemotaxis and/or Ca^{2+} mobilization (11, 13). An increase in the percentage of $CRTH2^+$ cells among cutaneous lymphocyte-associated Ag-positive and $CD4^+$ cells in blood was observed in patients with atopic dermatitis (14). The PGD_2-CRTH2 system is thus apparently involved in atopic dermatitis. However, the roles of CRTH2 in allergic inflammation, particularly in vivo, remain to be determined.

Atopic dermatitis is a common and distinctive chronic allergic disease that exhibits eosinophilia and increased IgE levels in blood. IgE has been shown to mediate immediate-type hypersensitivity via activation of mast cells, which release a series of chemical mediators including histamine and prostaglandins. Recent studies with murine models of skin inflammation have demonstrated that exogenous introduction of IgE or its gene induces immediate-type responses (ITRs) within a couple of hours, late-phase responses (LPRs) at 24 h, and very-late-phase responses (vLPRs)

*Department of Dermatology, Graduate School, Tokyo Medical and Dental University, Tokyo, Japan; [†]Department of Molecular Behavioral Biology, Osaka Bioscience Institute, Osaka, Japan; [‡]Department of Advanced Medicine and Development, Bio Medical Laboratories, Inc., Saitama, Japan; [§]Human Gene Sciences Center, Tokyo Medical and Dental University, Tokyo, Japan; [¶]Department of Comprehensive Pathology and Immunology, Tokyo Medical and Dental University, Tokyo, Japan; and [‖]Department of Microbiology and Immunology, Tohoku University Graduate School of Medicine, Sendai, Japan

Received for publication March 2, 2006. Accepted for publication May 16, 2006.

The costs of publication of this article were defrayed in part by the payment of page charges. This article must therefore be hereby marked *advertisement* in accordance with 18 U.S.C. Section 1734 solely to indicate this fact.

[1] This work was partially supported by grants from the Ministry of Education of Japan, the Cosmetology Research Foundation, and the Japan Society for the Promotion of Science.

[2] T.S. and R.M. contributed equally to this work.

[3] Address correspondence and reprint requests to Dr. Takahiro Satoh, Department of Dermatology, Graduate School, Tokyo Medical and Dental University, 1-5-45 Yushima, Bunkyo-ku, Tokyo 113-8519, Japan. E-mail address: tasa-1688.derm@tmd.ac.jp

[4] Abbreviations used in this paper: PGDS, PGD synthase; CRTH2, chemoattractant receptor homologous molecule expressed on Th2 cells; CHS, contact hypersensitivity; DC, dendritic cell; DP, PGD receptor; DNFB, 2,4-dinitrofluorobenzene; DTH, delayed-type hypersensitivity; ES, embryonic stem; H-PGDS, hemopoietic PGDS; ITR, immediate-type response; LC, Langerhans cell; LPR, late phase response; MDC, macrophage-derived chemokine; TARC, thymus- and activation-regulated chemokine; TNCB, 2,4,6-trinitrochlorobenzene; vLPR, very late phase response.

0022-1767/06/$02.00

(third-phase response) several days after challenge (15–18). Histopathological examination of vLPRs indicates epidermal hyperplasia and marked increases in lymphocyte and eosinophil cell numbers. These results clearly demonstrate the pathogenic involvement of IgE in chronic allergic inflammation as well as in ITR (15, 16). In addition, repeated challenge with haptens, the so-called chronic contact hypersensitivity (CHS) mouse model, induces an ITR followed by a late reaction with IgE elevation. These responses are accompanied by a cytokine shift from a Th1 profile to a Th2 profile (19, 20). The collective phenotypic appearance of these responses in mice resembles that of patients with atopic dermatitis.

To examine the link between CRTH2 and chronic allergic inflammation, we generated mice with targeted disruption of the *CRTH2* gene and used mouse models of skin inflammation. Our results demonstrate that CRTH2-mediated signals play essential roles in IgE-mediated cutaneous responses and chronic CHS and suggest the possibility that CRTH2 may be a potent therapeutic target for the treatment of chronic allergic skin inflammations such as atopic dermatitis.

Materials and Methods

Generation of CRTH2-deficient mice

Several genomic clones containing the *CRTH2* gene of the 129/sV mouse strain provided the 5′-*Nde*I-*Eco*RV 6.3-kb and 3′-*Dra*I-*Bgl*II 3.0-kb fragments, which were used as the left and right vector arms, respectively. The targeting vector was constructed by inserting the left arm, the neomycin cassette from ploxPneo-1, the right arm, and the diphtheria toxin cassette from pMC1DTpA (Kurabo) into the *Sma*I site, the *Eco*RI-*Xho*I sites, and *Kpn*I sites of pBluescript II, respectively, and it was then introduced into mouse embryonic stem (ES) cells (provided by Dr. S. Azuma, Kitasato University, Sagamihara, Japan) from the 129/sV mouse strain by electroporation. ES cells with homologous recombination were microinjected into C57BL/6J blastocysts. Male chimeras were crossed with BALB/cJ females to generate germline heterozygous offspring. After backcrossing with wild-type BALB/cJ for 10 generations, homozygous CRTH2 mutants and wild-type animals were obtained by intercrossing heterozygotes. Genotypes were determined by Southern blot hybridization or PCR. The use of animals was in full compliance with the Committee for Animal Experiments of Tokyo Medical and Dental University, Tokyo, Japan.

DNA preparation and Southern blot hybridization

Genomic DNA from mouse tails and ES cells was prepared as described previously (21) with some modifications, digested with restriction enzymes, electrophoresed in a 0.7% agarose gel, transferred to a nylon membrane, and hybridized with a 5′- or 3′-probe labeled with [α-^{32}P]dCTP (3000 Ci/mmol; Amersham Biosciences) at 55°C overnight. The membrane was washed three times in 2× SSC (3 M NaCl, 300 mM trisodium citrate) with 0.1% SDS at 65°C and subjected to autoradiography with a bioimaging analyzer (BAS 2000; Fuji Film).

RNA preparation and reverse transcription

Specimens were stored in RNA*later* (Ambion) at 4°C until use. Total cellular RNA from lung and skin was isolated using RNAeasy mini kit (Qiagen). Reverse transcription was conducted in a reaction buffer containing hexanucleotide mixture (A_{260}; 6.25 U/ml; Boehringer Mannheim), dNTPs (0.125 mM each), human placenta RNase inhibitor (80 U; Takara Bio), reverse transcriptase (400 U; Moloney murine leukemia virus; Takara Bio), and 800 ng of total RNA.

Polymerase chain reaction

PCR was conducted in a reaction buffer (10 mM Tris-HCl (pH 8.3), 50 mM KCl, 1.5 mM $MgCl_2$) containing dNTPs (2.5 mM each), 1 U/μl Perfect Match (Stratagene), and 5 U/μl *Taq* DNA polymerase (Takara Bio). The reaction was initiated by denaturation at 94°C for 3 min followed by 28 cycles for *GAPDH* and 33 cycles for *CRTH2* genes (1 min at 94°C, 1 min at 55°C, and 1 min at 72°C). Genomic DNA (~100 ng) or reverse-transcribed DNA (equivalent to 100 ng of total RNA) was used as a template. The primers used were: 5′-GAGCACGTACTCGGATGGAA-3′ and 5′-TCCTCGAGGCTACTTTTGC-3′ for the targeted mutant *CRTH2* gene;

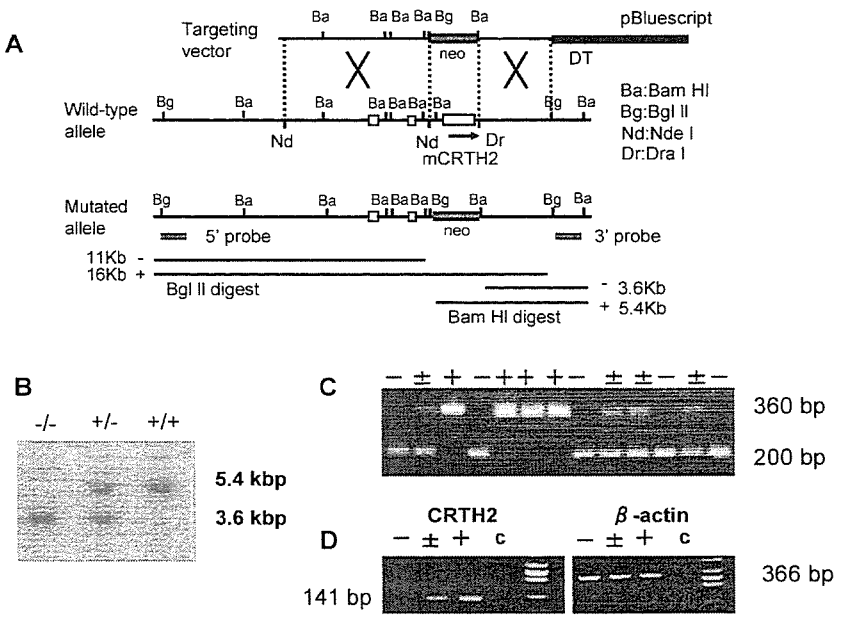

FIGURE 1. Targeted disruption of the *CRTH2* gene. *A*, Schematic representations of the targeting vector, wild-type allele, and mutant allele. Ba, Bg, Nd, and Dr indicate restriction sites for *Bam*HI, *Bgl*II, *Nde*I, and *Dra*I, respectively. Boxes on lines indicate regions that are transcribed. The 5′- and 3′-probes used for Southern blot analysis are shown. Lines with DNA sizes below the mutant allele indicate restriction fragments detected with either the 5′- or 3′-probe. Plus (+) and minus (−) signs indicate the wild-type and mutant alleles, respectively. *B*, Representative genomic Southern blot analysis for the wild-type (+/+) and mutant (−/−) homozygotes and the heterozygote (+/−). Genomic DNAs extracted from tails were digested with *Bam*HI and hybridized with the 3′-probe after gel separation and blotting. The 5.4- and 3.6-kb bands indicate the wild-type and mutant alleles, respectively. *C*, PCR genotyping of offspring from heterozygote intercrossing. The primer pairs used to detect the wild-type allele and the neomycin gene in the mutant allele generate 360- and 200-bp fragments, respectively. *D*, RT-PCR analysis of CRTH2 expression in lung. RNA was extracted from the lungs of wild-type (+) and mutant homozygotes (−) and heterozygotes (±) and subjected to RT-PCR with primers for CRTH2 and β-actin, generating 141- and 366-bp fragments, respectively. *Lane c*, control PCR without template.

5′-CGTAGCCGTGAGCCTGCGACTG-3′ and 5′-GGCGATTGCG GAGCCCACCACT-3′ for the wild-type *CRTH2* gene; 5′-AAATGGT GAAGGTCGGTGTG-3′ and 5′-TGAAGGGGTCGTTGATGG-3′ for GAPDH mRNA; 5′-CATGTGCTACTACAACTTGC-3′ and 5′-GCA GACTGAAGATGTGGTAGG-3′ for CRTH2 mRNA (22); and 5′-GGACTCCTATGTGGGTGACGAGG-3′ and 5′-GGGAGAGCATAGC CCTCGTAGAT-3′ for the β-actin gene (23). Mutant and wild-type alleles for CRTH2 gave rise to PCR-amplified fragments of 200 and 300 bp, respectively.

Cutaneous inflammatory reactions

IgE-mediated cutaneous reactions were induced by s.c. injection into the dorsal site of the mouse ear lobe with 1.25 μg of anti-DNP-specific IgE (MP Biomedicals). Mice were then challenged 24 h later with 20 μl of 0.2% 2,4-dinitrofluorobenzene (DNFB) (Nakarai Tesque) in acetone:olive oil (4:1). Ear thickness was determined using a dial thickness gauge (Peacock) before and after challenge. Ear swelling was expressed as the mean increase in thickness above the basal control value.

FITC (Sigma) in acetone:dibutyl phthalate (1:1) was used to induce allergic contact sensitivity by application of 100 μl of 1% solution onto ventral skin on day 0 and day 1. On day 6, ear lobes were challenged with 20 μl of 1% FITC. Ear thickness was determined immediately before and 24 h after challenge.

Chronic allergic contact hypersensitivity was induced by application of 50 μl of 5% 2,4,6-trinitrochlorobenzene (TNCB) (Nakarai Tesque) in ethanol:acetone (3:1) onto the ventral skin on day 0. On day 5, each ear lobe was challenged with 20 μl of 1% TNCB in acetone:olive oil (1:4). Application of 1% TNCB onto each ear lobe was repeated every 2 days from day 5 to day 25. Ear thickness was determined before and after each challenge.

Irritation dermatitis was induced by painting 20 μl of 1% croton oil (Nakarai Tesque) in acetone on mice ear lobes. Ear thickness was determined immediately before and 24 h after painting. Control ears were challenged with respective vehicles.

Delayed-type hypersensitivity (DTH) was induced by s.c. immunization with 100 μl of 20% SRBC in the back on day 0. On day 5, 20 μl of 20% SRBC was injected into the footpad. Footpad thickness was determined immediately before and 24 h after the challenge. Control groups were sensitized with PBS without SRBC.

Preparation and analysis of epidermal sheets

Mice were sacrificed, and each ear lobe was split into dorsal and ventral halves using forceps. The dorsal halves were cut into small pieces, and these were incubated for 2 h at 37°C in PBS containing 10 mM EDTA. The epidermis was peeled away from the dermis using forceps and then fixed in acetone for 5 min. Epidermal Langerhans cells (LC) were stained with goat polyclonal anti-Langerin Ab (Santa Cruz Biotechnology) using a Histofine SAB-PO kit (Nichirei).

Measurement of PGD_2 in the skin

The amount of PGD_2 in the skin was measured as described previously (24). Briefly, ear lobes were homogenized in 2 ml of ethanol containing 0.25 N HCl using a Polytron homogenizer. [^{3}H]PGD_2 (PerkinElmer) was added to each homogenate as a tracer to assess recovery during purification. An ethanol extract containing PGD_2 was added to Sep Pak C18 cartridges (Waters Associates), followed by elution with ethyl acetate and fractionation by HPLC. PGD2 was measured using an assay kit (Cayman Chemical).

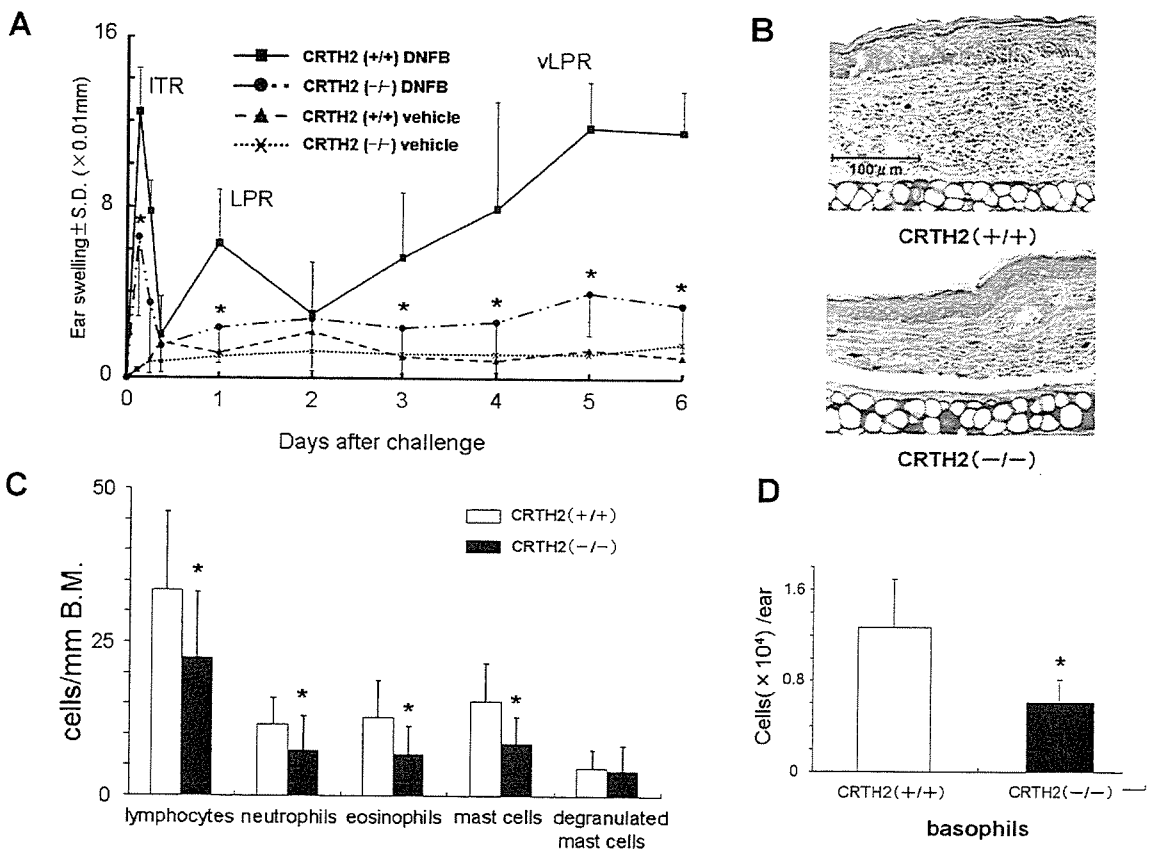

FIGURE 2. IgE-mediated cutaneous responses in CRTH2-deficient mice. *A*, Ear swelling induced by administration of Ag-specific IgE. Wild-type and CRTH2-deficient mice received DNP-specific IgE and were challenged with DNFB. Ear thickness was measured at the indicated times. *, $p < 0.05$. At least four mice for each group were used in the assay. *B*, Histopathological features of the skin during vLPR. Tissue sections of swollen ear lobes during vLPR from mutant and wild-type mice were prepared and subjected to Giemsa staining. (original magnification: ×200). *C*, Cell populations in infiltrates from inflammatory skin. Stained sections were observed by light microscopy to count the number of lymphocytes, neutrophils, eosinophils, and mast cells. B.M., basement membrane. *, $p < 0.05$. *D*, Basophils in inflammatory skin infiltrate. Single-cell suspensions from ear skin were stained with fluorescence-conjugated Abs for FcεRI, c-*kit*, and Gr-1 and analyzed by flow cytometry. Cells with FcεRI and without c-*kit* and Gr-1 were counted as basophils. Representative results from three independent experiments are shown. Error bars indicate SD.

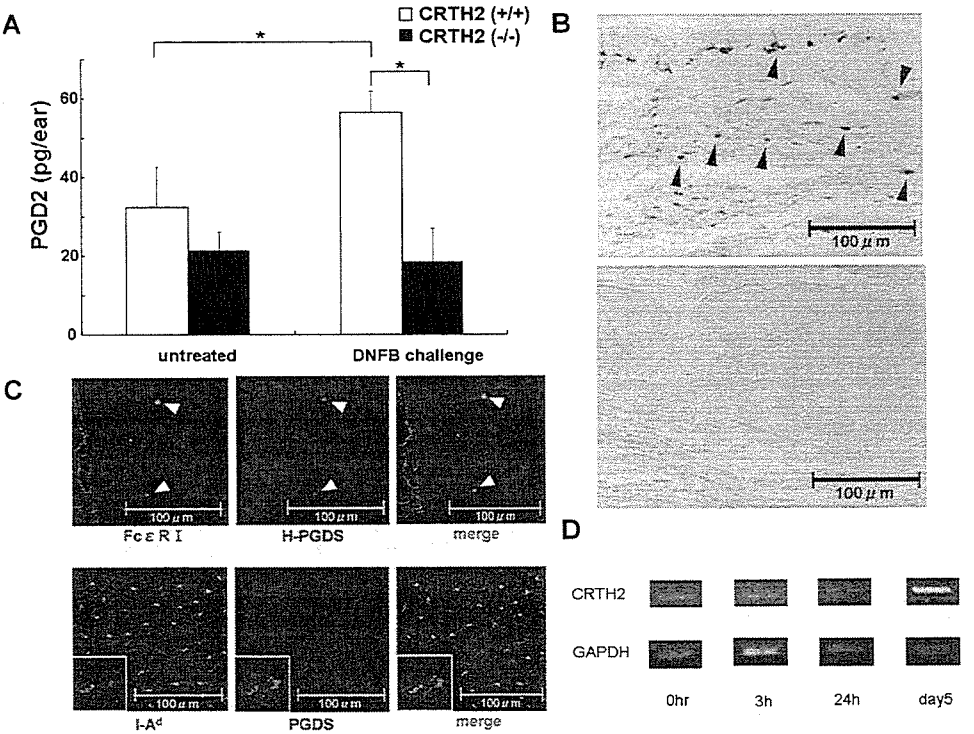

FIGURE 3. PGD_2 production and CRTH2 expression during inflammatory responses. *A*, PGD_2 production before and after challenge. CRTH2-deficent and wild-type mice were sensitized with DNP-IgE and challenged with DNFB. On day 5, ear lobes were frozen in liquid nitrogen, homogenized, and extracted with ethanol. After purification, the amounts of PGD_2 were measured with an assay kit. *, $p < 0.05$. *B*, H-PGDS$^+$ cells in the skin at vLPR (*upper panel*). Ear tissues were stained with anti-H-PGDS Ab and anti-rabbit IgG Ab and examined by microscopy. Arrowheads indicate cells positive for H-PGDS (original magnification, ×400). *Lower panel*, negative control staining. *C*, Expression of FcεRI or MHC class II in H-PGDS$^+$ cells in the skin. Tissue sections from normal (*lower panels*) and inflammatory skin (*upper panels*) were stained with anti-I-A^d Ab and anti-FcεRIα Ab, respectively, in addition to anti-H-PGDS Ab, and were subjected to confocal laser-scanning microscopic analysis. Arrowheads indicate cells positive for respective molecules. (original magnification: *upper panel*, ×200; *lower panel*, ×400). *D*, Expression of CRTH2 during inflammation of challenged skin. RNA was extracted from the skin of wild-type mice before and after challenge and subjected to RT-PCR with a set of primers specific for CRTH2 (*upper panel*) and GAPDH (*lower panel*).

Immunohistochemistry for hemopoietic PGDS (H-PGDS)

Tissue sections were deparaffinized, rehydrated, and incubated in absolute methanol with 0.3% H_2O_2 to inactivate endogenous peroxidase activity. After treatment with trypsin, sections were incubated in PBS containing 10% normal goat serum, 0.01% Triton X-100, and 0.1% NaN_3 and treated with rabbit polyclonal anti-mouse H-PGDS Ab (raised in Osaka Bioscience Institute), followed by incubation with biotinylated anti-rabbit IgG and Vectastain ABC reagent (Vector Laboratories). In some experiments, frozen tissue sections were incubated with anti-mouse H-PGDS Ab followed by incubation with tetramethylrhodamine isothiocyanate-conjugated anti-rabbit IgG (DakoCytomation). The sections were then incubated with FITC-conjugated anti-CD4 Ab (clone RM4-5; BD Biosciences), anti-CD8α Ab (clone 53-6.7; BD Biosciences), or anti-FcεRIα Ab (clone MAR-1; eBioscience). For double staining of LC, epidermal sheets were first stained with FITC-conjugated anti-I-A^d Ab (clone AMS-32.1; BD Biosciences) followed by H-PGDS staining. Immunostained samples were examined under a confocal laser-scanning microscope (FluoView; Olympus).

Flow cytometric analysis of murine basophils in the skin

Cells were obtained from ears by treatment with collagenase type 3 (115 U/ml; Worthington Biochemical) and stained with FITC-conjugated anti-mouse FcεRIα Ab (MAR-1), R-PE-conjugated anti-mouse CD117 (c-*kit*) Ab (ACK45; BD Biosciences), and/or PE-Cy5.5-conjugated anti-mouse Gr-1 Ab (clone RB6-8C5; BD Biosciences) and subjected to flow cytometric analysis. Cells positive for FcεRIα and negative for both c-*kit* and Gr-1 were considered to be basophils (25).

In vivo migration of LC and DC

Draining lymph node cells were collected from mice sacrificed 24 h after the application of 1% FITC to the ventral skin. Cells were incubated with PE-conjugated anti-mouse CD11c Ab (BD Biosciences) and analyzed with a flow cytometer.

Measurement of cytokines and chemokines in the skin

Punched ear lobes (8-mm diameter) from challenged mice were homogenized in PBS containing 0.1% Tween 20 (500 μl/tissue) and then centrifuged at 15,000 × *g* for 10 min. Concentrations of cytokines and chemokines in the supernatants were determined by sandwich ELISA. ELISA kits for murine IL-4, IL-5, and IFN-γ were purchased from Pierce, and the ELISA kits for IL-13, thymus- and activation-regulated chemokine (TARC), macrophage-derived chemokine (MDC), RANTES, and IFN-γ-inducible protein 10 were from R&D Systems. The eotaxin enzyme immunoassay kit was obtained from Techne Laboratories.

Measurement of IgE levels in serum

Peripheral blood was obtained from the retroorbital plexus. Serum IgE levels were determined using a commercial sandwich ELISA kit (Yamasa) according to the manufacturer's instructions.

Statistical analyses

Student's *t* test was used to assess the statistical significance of differences between mean values. Statistical analyses of the results in Fig. 5 were performed by the Bonferroni multiple comparison test.

Results

Generation and general properties of CRTH2-deficient mice

Mice lacking the *CRTH2* gene were generated by targeted disruption of the *CRTH2* gene (Fig. 1*A*). Germline-transmitting chimeras were mated with wild-type BALB/c females, and CRTH2 heterozygotes were then backcrossed with BALB/c 10 times. The

resultant heterozygotes were intercrossed to generate CRTH2 homozygous mutant, heterozygous mutant, and wild-type animals. Genotypes were determined by Southern blot hybridization and PCR (Fig. 1, *B* and *C*). Offspring from heterozygote intercrosses were born at approximately the expected Mendelian ratios (57 wild-type, 145 heterozygote, and 51 homozygote mice) (1:2.5:0.9). RT-PCR analysis for CRTH2 mRNA showed little or no expression of CRTH2 transcripts in homozygotes in lungs in which CRTH2 mRNA was detected in wild-type animals (Fig. 1*D*). CRTH2-deficient homozygotes showed no significant abnormalities at birth or during postnatal growth. Intercrosses between mutant homozygotes yielded normal numbers of offspring, indicating that the CRTH2-deficient homozygotes were fertile.

IgE-mediated cutaneous responses in CRTH2-deficient mice

Mouse responses of IgE-mediated cutaneous inflammation have been shown to consist of at least three phases, ITR, LPR and vLPR, together with marked infiltration by eosinophils and lymphocytes (15–18). To examine the involvement of CRTH2 in IgE-mediated cutaneous responses in vivo, we assessed the ear-swelling responses of CRTH2-deficient mice. Mice were passively immunized with DNP-specific IgE and challenged with DNFB. The ear-swelling response after challenge was clear in wild-type mice, but all three phases of the response were significantly reduced in mutant mice (Fig. 2*A*). Among the three phases, the mostly marked reduction was seen for vLPR compared with wild-type mice (65%). Histological analyses of the challenged ears of CRTH2-deficient mice on day 5 showed a profound reduction in dermal cellular infiltrate when compared with wild-type mice (Fig. 2*B*). Similar reductions in ear swelling were seen in the CRTH2-deficient C57BL/6 strain (data not shown). These observations indicate that CRTH2 functions in the cutaneous responses induced by Ag-specific IgE.

The infiltrate included lymphocytes, eosinophils, neutrophils, and mast cells. These cell types were significantly decreased in the infiltrates of mutant mice in terms of cell number (Fig. 2, *B* and *C*). In humans, the CRTH2-mediated signal induces chemotaxis in basophils (11). In mice, basophils play a critical role in 2,4,6-trinitrophenyl-IgE-mediated cutaneous vLPR (25). We thus investigated the effects of CRTH2 on basophil recruitment to the skin. Flow cytometric analysis of dermal cells in vLPR demonstrated that basophil infiltration was also significantly reduced in mutant mice (Fig. 2*D*).

We then examined the production of PGD_2 in the challenged ear lobes of CRTH2-deficient and wild-type mice. Challenge with DNFB resulted in a significant increase in PGD_2 levels in wild-type mice on day 5 (vLPR), whereas mutant mice did not show any appreciable elevation of PGD_2 (Fig. 3*A*). A significant difference in PGD_2 levels at 3 and 24 h after challenge was not observed between mutant and wild-type mice (data not shown). Cells expressing H-PGDS were present during IgE-induced vLPR (Fig. 3*B*). H-PGDS expression in the dermis was seen in cells positive for FcεRI (Fig. 3*C*), CD4, or CD8 (data not shown) by confocal laser-scanning microscopy. Moreover, H-PGDS was constitutively expressed in MHC class II-positive epidermal LC (Fig. 3*C*). Ag challenge may stimulate $Fc\varepsilon RI^+$ cells, T cells, and LC to produce PGD_2, which, together with other chemical mediators, contributes to recruitment of $CRTH2^+$ cells into inflammatory sites. Indeed, levels of CRTH2 mRNA in the skin were low but detectable before challenge and increased with time after challenge (Fig. 3*D*). This notion is consistent with the results observed in wild-type mice that were administered either HQL-79 (Cayman Chemical), an inhibitor of PGD synthase, or ramatroban (Bayer Yakuhin), an antagonist of CRTH2. Wild-type BALB/c mice were perorally administered with HQL-79 for 8 consecutive days (days −1 to 6) and immunized with DNP-specific IgE. vLPR was markedly inhibited by administration of HQL-79 (Fig. 4*A*). Similar results were seen with mice orally given ramatroban at a dose of 0.3 mg/kg (Fig. 4*B*). Collectively, these results demonstrate that PGD_2 is involved in the pathogenesis of IgE-mediated cutaneous inflammation via CRTH2.

Cytokine and chemokine production in CRTH2-deficient mice

To gain insight into CRTH2-mediated inflammatory responses, we determined the production of cytokines and chemokines in skin lesions. The homogenates of swollen ears were subjected to measurement of IL-4, MDC, eotaxin, IFN-γ, RANTES, and TARC. IL-4 and IFN-γ production in CRTH2-deficient mice was comparable to that in wild-type mice. Levels of MDC and RANTES 6 days after challenge were significantly lower in CRTH2-deficient mice than in wild-type mice (Fig. 5). CRTH2-deficient mice produced lower levels of eotaxin than wild-type mice on day 6; however, this was not statistically significant. Three hours after challenge, mutant mice exhibited higher TARC production; however,

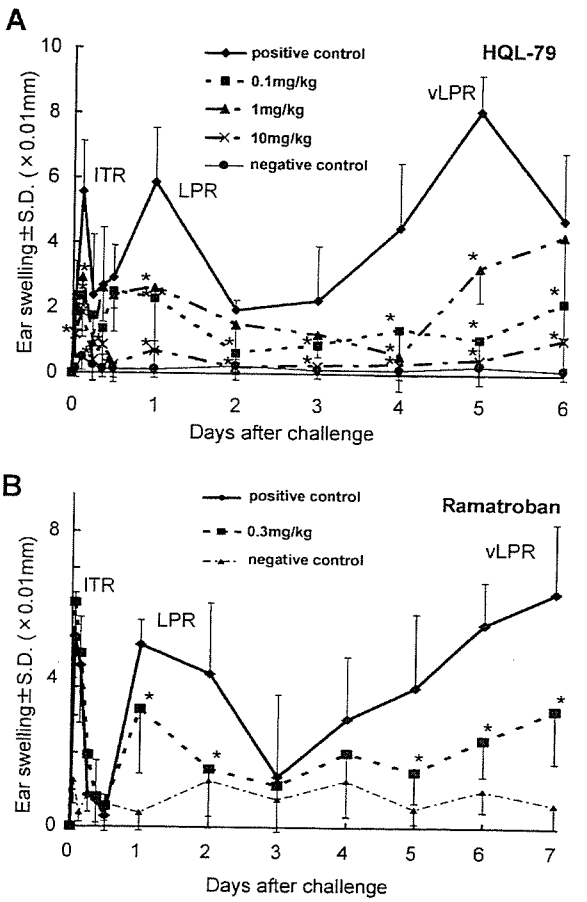

FIGURE 4. Involvement of PGD_2 and CRTH2 in IgE-mediated cutaneous responses. *A*, Effects of HQL-79 on ear swelling induced by IgE. Wild-type mice were sensitized with DNP-IgE on day −1 and challenged by DNFB painting on day 0. HQL-79 was administered from day −1 to day 6 at the doses indicated in the figure, and ear thickness was determined at the indicated times. *, $p < 0.05$, as compared with positive control. *B*, Effect of ramatroban on IgE-mediated cutaneous responses. Wild-type mice were sensitized with DNP-specific IgE and challenged with DNFB. Ramatroban was administered at doses of 0.3, 3, and 30 mg/kg body weight for 8 days. Ear thickness was measured at the indicated times after challenge. Mice administered 3 and 30 mg/kg exhibited similar results. *, $p < 0.05$. Each group consisted of at least four mice.

afterward the differences were not significant. IL-5, IL-13, and IFN-γ-inducible protein 10 were undetectable in cutaneous preparations from both strains (data not shown). CRTH2-deficient mice exhibited defects in cytokine and chemokine production, and these defects were not biased toward Th2-type cytokines and chemokines.

Acute CHS in CRTH2-deficient mice

Because acute CHS to FITC is Th2 dependent (26) and is sensitive to the CRTH2 antagonist ramatroban (27), we examined the involvement of CRTH2 in CHS to that of FITC. CHS was induced in CRTH2-deficient mice by sensitization with FITC. Both mutant and wild-type mice showed FITC-induced CHS; however, ear swelling in mutant mice was slightly but significantly alleviated (Fig. 6*A*).

We then attempted to determine whether CRTH2 is involved in the migration of epidermal LC and DC in the afferent phase of FITC-induced CHS. In untreated skin, the number of LC in the epidermis of CRTH2-deficient mice was comparable to that in wild-type mice (Fig. 6*B*). Upon application of FITC, the number of $FITC^+$ LC and DC with CD11c in regional lymph nodes increased, but no significant differences were seen between mutant and wild-type mice as assessed by flow cytometry; the percentage of LC and DC among total cells in lymph nodes was 0.5 ± 0.088% in wild-type mice and 0.67 ± 0.131% in CRTH2-deficient mice, thus demonstrating that the reductions in acute CHS in CRTH2-deficient mice are not due to impaired LC and DC migration into regional lymph nodes during sensitization. This finding indicates that CRTH2 is not involved in LC migration, which agrees with the previous observation that PGD_2 affects LC migration via DP (9).

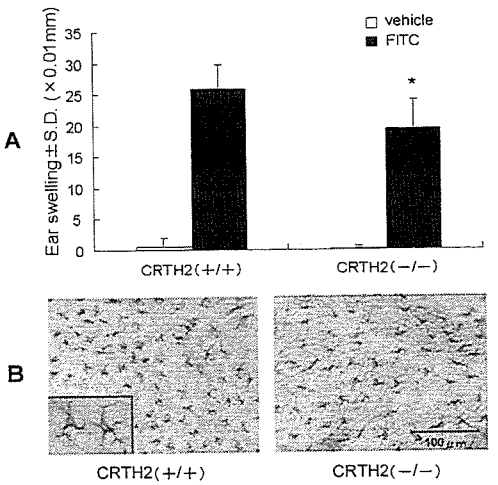

FIGURE 6. Acute CHS induced by FITC administration. *A*, Ear swelling in FITC-induced acute CHS. Mice were sensitized with FITC on the ventral skin on days 0 and 1 and challenged with FITC on day 6. Ear thickness was measured 24 h after challenge. Four mice were used in each group, and representative results among three separate experiments are shown. *, $p < 0.05$. *B*, Histological analysis of epidermal LC. Untreated epidermis from mutant and wild-type mice was stained with anti-Langerin Ab and observed by light microscopy. The number of epidermal LC in CRTH2-deficient and wild-type mice was 1451.2 ± 203.79 and 1468.8 ± 204.18 cells/mm^2, respectively (original magnification, ×400).

Chronic CHS in CRTH2-deficient mice

Repeated application of hapten has been shown to induce chronic CHS, exhibiting an ITR instead of a delayed-type response and a

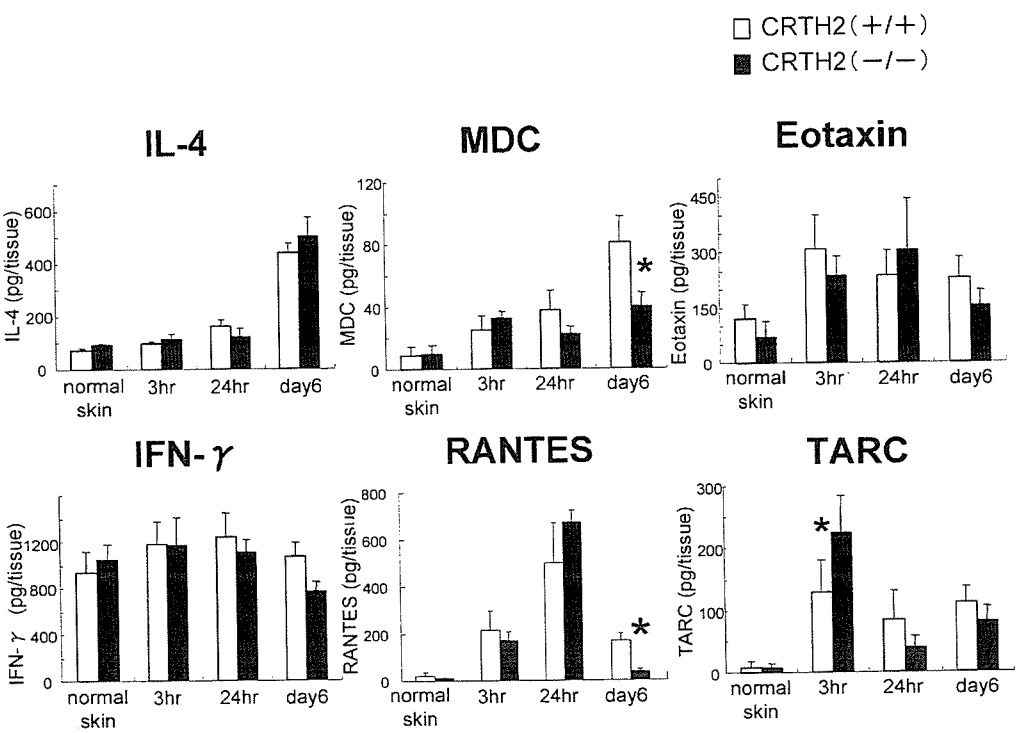

FIGURE 5. Levels of cytokines and chemokines during cutaneous responses. Mutant and wild-type mice were challenged with DNFB following DNP-IgE injection, At the indicated times after challenge, ear skin specimens were collected by punching, and supernatants were prepared from skin homogenates. Amounts of cytokines and chemokines in the supernatants were determined by ELISA. One group at each time point consisted of 3–5 animals. Representative results from two independent experiments are shown. Data were analyzed by the Bonferroni multiple comparison test. *, $p < 0.05$. Error bars indicate SD.

shift in local cytokine production from a Th1 to a Th2 profile (19, 20, 28). To investigate the effects of CRTH2 on chronic CHS, mutant and wild-type mice were challenged with TNCB every 2 days from day 5 to day 25 following initial sensitization on day 0. Both strains exhibited similar shifts in the kinetics of cutaneous reactions. As seen with the acute-phase responses to FITC shown in Fig. 6*A*, ear-swelling responses 24 h after challenge on day 5 (acute CHS) were slightly weaker in CRTH2-deficient mice than in wild-type mice (Fig. 7*A*). Mutant mice exhibited reduced cutaneous reactions in chronic CHS in response to challenge on days 13 and 25 (Fig. 7*A*). Basal ear thickness increased gradually with challenge. This phenomenon is thought to result from accumulated inflammation induced by repeated challenge. The basal levels of the ear thickness in mutant mice on day 27 were significantly reduced when compared with those in wild-type mice (Fig. 7*B*). The levels of total serum IgE on day 27 in TNCB-induced CHS were significantly higher in wild-type mice than in CRTH2-deficient mice (Fig. 7*C*). These results imply that CRTH2 participates in the development of hapten-induced chronic CHS.

Effects of CRTH2 on DTH reaction and irritation dermatitis

The pathomechanisms of IgE-mediated cutaneous responses and chronic CHS in which tissue eosinophilia is prominent may be different from those of DTH reaction or irritation dermatitis. Based on the observation that the DTH reaction on the footpad in response to SRBC is independent of Th2-type response (29), we speculated that CRTH2 is not involved in the DTH reaction. Mutant mice administered SRBC exhibited significant footpad responses that were similar to those of wild-type mice (Fig. 8*A*).

Irritation dermatitis is dependent on mast cell-derived mediators (30); thus, we further examined whether the PGD_2-CRTH2 system is involved in this dermatitis. Irritation dermatitis was induced by the application of croton oil, and ear swelling was compared between the two mouse strains. Interestingly, the lack of CRTH2 had no effect on the ear-swelling response to croton oil application in the two strains (Fig. 8*B*), which is presumably consistent with the previous observation that croton oil dermatitis is not dependent on Th2-mediated signals (29). These observations suggest that DTH and irritation dermatitis are mediated by cells that do not require CRTH2 function.

Discussion

PGD_2 has been implicated in allergic reactions. This notion is based on the observations that overexpression of PGDS induces Th2-dominated lung inflammation with pronounced eosinophilia (6) and that *DP* gene disruption results in relief of allergic asthma (10). In addition, the activation of CRTH2 has been shown to aggravate allergic lung inflammation (22). However, the role of CRTH2 in allergic reactions remains uncertain.

In the present study, using CRTH2-deficient mice we clearly demonstrate for the first time that the PGD_2-CRTH2 system plays a role in the IgE-mediated inflammatory response in the skin. CRTH2-deficient mice exhibited reduced skin responses. This reduced effect was most marked during vLPR. The same reduction was seen in mice administered the PGDS inhibitor HQL-79 or the CRTH2 antagonist ramatroban. These results unequivocally show that CRTH2 mediates IgE-dependent cutaneous inflammation. It is possible that DP may also be cooperatively involved in this event.

Histological analysis revealed reductions in the number of lymphocytes, eosinophils, neutrophils, and mast cells in infiltrates. In addition, basophil infiltration in the dermis was also reduced during vLPR in mutant mice. These observations indicate that various cells are affected by *CRTH2* gene disruption. PGD_2 may act as an attractant for a panel of cells positive for CRTH2. Alternatively,

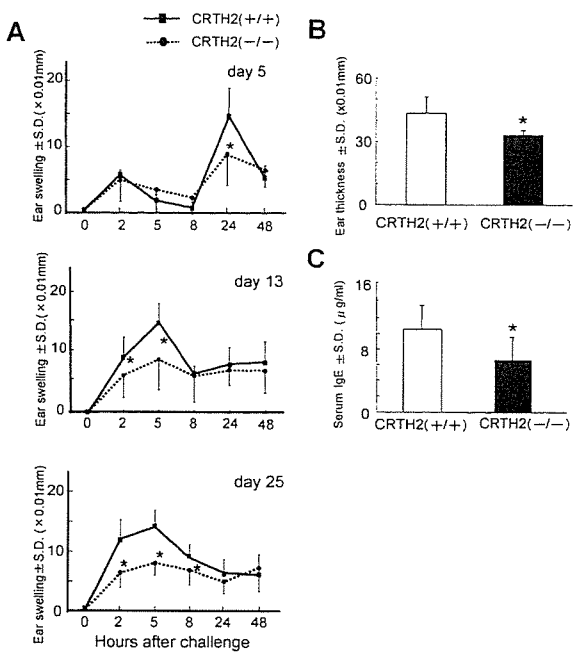

FIGURE 7. Involvement of CRTH2 in chronic CHS induced by TNCB. *A*, Kinetics of ear swelling in response to challenge. Mutant and wild-type mice were sensitized with TNCB on the ventral skin on day 0 and challenged every 2 days, from day 5 to day 25. Ear swelling was determined at the indicated times after challenge on day 5, day 13, and day 25. *B*, Challenge-dependent increases in basal levels of ear thickness. Ear thickness was determined at 48 h after final challenge (day 27). *C*, Levels of serum IgE. Concentration of IgE in sera was determined by ELISA. Results are shown as averages ± SD of at least four mice in each group. *, $p < 0.05$.

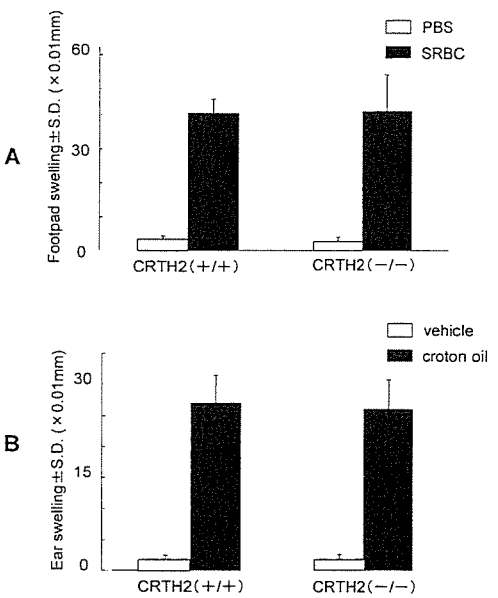

FIGURE 8. Effects of CRTH2 in DTH and irritation dermatitis. *A*, Effects of CRTH2 on SRBC-induced DTH. Mice were sensitized with SRBC in the back and measured for footpad thickness at 24 h after challenge with SRBC at the footpad. As controls, mice received PBS instead of SRBC suspension. *B*, Effects of CRTH2 on croton oil-induced irritation dermatitis. Ear lobes were painted with 1% croton oil, and ear thickness was determined. Control mice were painted with acetone instead of croton oil. Experiments were repeated three times. Each group consisted of at least four mice.

CRTH2 may attract the first basophils during the early stages of skin inflammation, which then induces a further cascade of cell recruitment. A recent study illustrates that basophils are critical in the induction of 2,4,6-trinitrophenyl-IgE-mediated vLPR (25). Our results showing that mutant mice exhibited less ear swelling in response to DNP-specific IgE may be attributed, at least in part, to impaired basophil infiltration. This impairment is presumably associated with a lack of CRTH2-mediated signals.

PGD_2 produced by allergic stimulation attracts CRTH2-positive cells, which include cells positive for H-PGDS, into inflammation sites. These cells were identified as $Fc\varepsilon RI^+$ mast cells or basophils and $CD4^+$ and $CD8^+$ cells seen during vLPR in the dermis (Fig. 3*B*) and are presumably the sources of the high levels of PGD_2 during vLPR (Fig. 3*A*), which may further induce infiltration. This notion is consistent with the recent finding that 13,14-dihydro-15-keto-PGD_2, which is a CRTH2 agonist, exacerbates skin inflammation induced by OVA (22).

We observed constitutive expression of H-PGDS in epidermal resident LC, as shown in the rat skin in which LC express PGDS (31). Constitutive expression of H-PGDS may contribute to basal levels of PGD_2, which acts to recruit CRTH2-positive inflammatory cells into the skin for surveillance even under normal conditions. A recent report demonstrates that, under allergic conditions, IgE-mediated activation of mast cells induces LC migration toward lymph nodes in vivo (32). LC in lymph nodes may be potent sources of PGD_2 for $CRTH2^+$ cell homing, after which the cells migrate to inflammatory sites during IgE-mediated cutaneous responses.

Our results with CRTH2-deficient mice imply that CRTH2 may participate in the constitution of local cytokine and chemokine profiles in allergic inflammation. Mutant mice differed from wild-type mice in the production of MDC and RANTES induced by hapten challenge. The impaired recruitment of eosinophils may be due not only to the direct effects of the absence of PGD_2-CRTH2 signaling but also to diminished production of RANTES. Although IL-5 levels in our ear specimens were below the detection limit, IL-5 may not be the cause of impaired cell recruitment, as IL-5 is reported to be unnecessary for eosinophil recruitment into the skin (33). It also appears likely that the reduced lymphocyte accumulation is partly associated with decreased MDC and RANTES production. In humans, CRTH2 is preferentially expressed in Th2 cells rather than in Th1 cells, thus resulting in elevated production of IL-4, IL-5, and IL-13 in human T cells by CRTH2 stimulation (34). Thus, one may assume that the disruption of the *CRTH2* gene causes a shift from Th2 to Th1 cytokine and chemokine profiles in mice. Expression of CRTH2 in mice, however, is not biased toward Th2 cells, unlike the case in humans (35). Indeed, production of IL-4 and IFN-γ was not affected by the absence of CRTH2. In other words, changes in local cytokine and chemokine levels in CRTH2-deficient mice cannot simply be explained by impaired infiltration of Th2 cells. Our results suggest that the cytokines and chemokines regulated by CRTH2 are different in mice and humans.

Experimental chronic CHS is established by repeated application of hapten. Each application induces ear swelling, which occurs at earlier time points than those by other applications. In the present study, no differences were observed in the shift of ear swelling kinetics; however, the ear swelling in CRTH2-deficient mice was lower than that in wild-type mice. The differences appeared predominantly in the basal thickness of ears, which increased gradually after each application. Basal thickness in mutant mice was three-quarters that of wild-type mice on day 27. Mutant mice appeared to produce lower levels of IgE in sera than wild-type mice. At present, a functional link between CRTH2 and IgE level is unclear. Chronic CHS in mice is thought to be representative of human atopic dermatitis. This model is histologically characterized by epidermal hyperplasia and marked increases in dermal eosinophils (19, 20). These findings suggest that CRTH2 is a potential target for therapeutic improvement of chronic eczematous reactions.

The absence of CRTH2 suppressed acute CHS induced by either TNCB or FITC application. Similar suppression was also seen in FITC-mediated acute CHS in mice treated with ramatroban (27). The suppressive effects caused by ramatroban appeared to be greater than those observed with dysfunction of CRTH2. This observation might be attributable to the action of ramatroban on a thromboxane A2 receptor other than CRTH2. However, this may not be case, as a thromboxane A2 receptor antagonist had no effect on the responses. Alternatively, targeted disruption of the *CRTH2* gene may have resulted in activation of alternative pathways, such as the DP receptor pathway, that may be partly able to compensate for the lack of the CRTH2-derived signals. This notion is supported by the recent study that, in an asthmatic model, DP signals appear to regulate production of Th2 cytokines (10).

After completion of this study, another study using an asthma model with CRTH2-deficient C57BL/6 mice reported enhanced eosinophil recruitment into the lung and production of IL-5 and IL-13 by splenocytes (36). Our preliminary asthma experiments did not show significant difference in infiltrates in the lung between our mutant and wild-type C57BL/6 mice (H. Hirai, unpublished results). In addition, we observed that splenocytes of mutant C57BL/6 mice produced the same amounts of IL-4, IL-5, and IFN-γ as those in wild-type mice upon CD3/CD28 stimulation. Similar results were seen in BALB/c background mice. At present, we do not know the reason for this inconsistency between the two groups, each of which established CRTH2-deficient mice independently. To draw final conclusions, further study including experiments with antagonists and agonists for CRTH2 will be required.

In summary, the present study shows that PGD_2-CRTH2 interaction plays important roles in the development of chronic allergic inflammation in the skin, such as IgE-mediated vLPR and chronic CHS, and that CRTH2 is not involved in irritation dermatitis. CRTH2 may thus have potential as a therapeutic target for treatment of atopic dermatitis and other allergic skin diseases.

Acknowledgments

We thank S. Azuma for ES cells and K. Ohbo for useful comments. We are also grateful to M. Sekiya, Y. Nakano, and E. Matsumoto for technical assistance.

Disclosures

The authors have no financial conflict of interest.

References

1. Whittle, B. J., S. Moncada, and J. R. Vane. 1978. Comparison of the effects of prostacyclin (PGI2), prostaglandin E1 and D2 on platelet aggregation in different species. *Prostaglandins* 16: 373–388.
2. Nagoshi, H., Y. Uehara, F. Kanai, S. Maeda, T. Ogura, A. Goto, T. Toyo-oka, H. Esumi, T. Shimizu, and M. Omata. 1998. Prostaglandin D2 inhibits inducible nitric oxide synthase expression in rat vascular smooth muscle cells. *Circ. Res.* 82: 204–209.
3. Narumiya, S., and N. Toda. 1985. Different responsiveness of prostaglandin D2-sensitive systems to prostaglandin D2 and its analogues. *Br. J. Pharmacol.* 85: 367–375.
4. Beasley, C. R., C. Robinson, R. L. Featherstone, J. G. Varley, C. C. Hardy, M. K. Church, and S. T. Holgate. 1987. 9α,11β-Prostaglandin F2, a novel metabolite of prostaglandin D2, is a potent contractile agonist of human and guinea pig airways. *J. Clin. Invest.* 79: 978–983.
5. Miadonna, A., A. Tedeschi, C. Brasca, G. Folco, A. Sala, and R. C. Murphy. 1990. Mediator release after endobronchial antigen challenge in patients with respiratory allergy. *J. Allergy Clin. Immunol.* 85: 906–913.
6. Fujitani, Y., Y. Kanaoka, K. Aritake, N. Uodome, K. Okazaki-Hatake, and Y. Urade. 2002. Pronounced eosinophilic lung inflammation and Th2 cytokine